



Cite this: *RSC Adv.*, 2022, 12, 19512

# Synthesis of MoS<sub>2</sub>-based nanostructures and their applications in rechargeable ion batteries, catalysts and gas sensors: a review

Wei Sun,<sup>id ac</sup> Yaofang Zhang,<sup>\*ac</sup> Weimin Kang,<sup>id ad</sup> Nanping Deng,<sup>ad</sup>  
Xiaoxiao Wang,<sup>ad</sup> Xiaoying Kang,<sup>ac</sup> Zirui Yan,<sup>ac</sup> Yingwen Pan<sup>ac</sup> and Jian Ni<sup>b</sup>

Molybdenum disulfide (MoS<sub>2</sub>) is a two-dimensional (2D) layered material with a graphene-like structure that has attracted attention because of its large specific surface area and abundant active sites. In addition, the compounding of MoS<sub>2</sub> with other materials can enhance the performance in applications such as batteries, catalysts, and optoelectronic devices, etc. MoS<sub>2</sub> is prepared by various methods, among which chemical deposition and hydrothermal methods are widely used. In this review, we focus on summarizing the applications of MoS<sub>2</sub> and MoS<sub>2</sub> composite nanomaterials in rechargeable ion batteries, catalysts for water splitting and gas sensors, and briefly outline the preparation methods.

Received 8th March 2022

Accepted 17th June 2022

DOI: 10.1039/d2ra01532c

rsc.li/rsc-advances

## 1. Introduction

Nanomaterials have attracted increasing research interest as a result of its fascinating physicochemical properties, such as the nano-size effect and large specific surface area. In 2005, the emergence of monolayer graphene set off a research boom in 2D materials.<sup>1–3</sup> Many novel 2D materials have also been developed, such as hexagonal boron nitride (hBN) and transition metal dichalcogenides (TMDs). They are widely used in energy, sensing and other applications due to their excellent physical and chemical properties.<sup>4–9</sup> Notably, MoS<sub>2</sub>, a member of TMDs, is a promising 2D material among compounds with graphene-like structures.

It is well known that MoS<sub>2</sub> materials have a wide range of applications, and we found that it has a high proportion of catalysts, batteries and gas sensors applications by searching the Web of Science for articles related to the applications of MoS<sub>2</sub> in the last decade (Fig. 1b). Fig. 1a summarizes the number of published SCI papers on MoS<sub>2</sub> over the last decade (up to May 2022) in the batteries, catalysts, and gas sensors. It is clear that MoS<sub>2</sub> is attracting more and more attention in these applications.

MoS<sub>2</sub> exhibits unique advantages over graphene-based or hBN-based nanomaterials in these applications. In detail, in

batteries, MoS<sub>2</sub> is used as an electrode material due to its high specific surface area and unique layer-like structure.<sup>10</sup> In catalysts, MoS<sub>2</sub> is a promising alternative to the precious metal Pt catalysts for hydrogen reaction evolution (HER) and

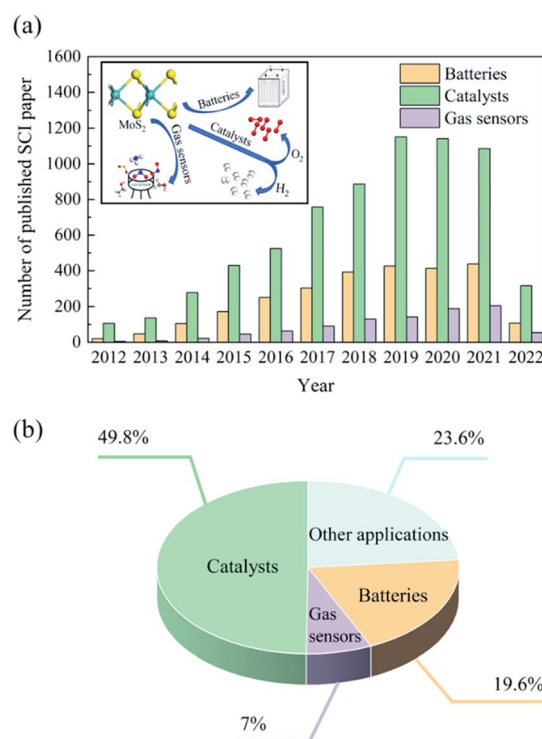


Fig. 1 (a) Statistics of MoS<sub>2</sub> core publications in batteries, catalysts, and gas sensors. (b) Percentage of core publications of MoS<sub>2</sub> in different applications in the last decade (up to May 2022).

<sup>a</sup>State Key Laboratory of Separation Membranes and Membrane Processes, Tiangong University, Tianjin 300387, PR China

<sup>b</sup>Department of Electronic Science and Technology, College of Electronic Information and Optical Engineering, Nankai University, Tianjin, 300350, China

<sup>c</sup>School of Physical Science and Technology, Tiangong University, Tianjin 300387, PR China

<sup>d</sup>School of Textile Science and Engineering, Tiangong University, Tianjin 300387, China



photocatalytic water splitting, while  $\text{MoS}_2$  can be used in combination with other materials to improve visible light catalytic activity for the degradation of organic pollutants in industrial wastewater.<sup>11,12</sup> In terms of gas-sensitive properties,  $\text{MoS}_2$  has good responsiveness and selectivity to some gases at room temperature (RT), which has led to widespread research and application of  $\text{MoS}_2$  materials in gas sensors.<sup>13</sup>

Recent years, many reviews about  $\text{MoS}_2$  nanomaterials were published. Some researchers have reviewed the application and preparation of  $\text{MoS}_2$  in energy (such as batteries and catalysts),<sup>14–16</sup> some have reviewed the application and preparation of  $\text{MoS}_2$  in electronic components (such as memristors and field-effect transistors),<sup>17–20</sup> some focus on  $\text{MoS}_2$  for detection and sensing applications,<sup>21–23</sup> some have listed in detail the synthesis and application of 1T  $\text{MoS}_2$ ,<sup>24–26</sup> and others have focused on the synthesis method of  $\text{MoS}_2$ .<sup>27</sup> Based on the previous researches and summaries, in this review, we comprehensively and systematically describe the applications of  $\text{MoS}_2$  and  $\text{MoS}_2$ -based composites in rechargeable ion batteries, catalysts and gas sensors in recent years, and summarize the corresponding preparation schemes.

## 2. Applications and synthesis strategies of $\text{MoS}_2$ in rechargeable ion batteries

To meet future energy storage needs, rechargeable ion batteries based on  $\text{Li}^+$ ,  $\text{Na}^+$ ,  $\text{Al}^{3+}$  and  $\text{Zn}^{2+}$  have been widely studied and prepared.<sup>28–31</sup>  $\text{MoS}_2$  has a layered structure, which are connected by van der Waals forces with weak interlayer interactions and large layer spacing.<sup>32</sup> High theoretical capacity, high charging rate and excellent stability make  $\text{MoS}_2$  become a promising electrode material. In this work, we will focus on the application and preparation of  $\text{MoS}_2$  as electrode materials.

### 2.1 Lithium-ion batteries

Using  $\text{MoS}_2$  or composites of  $\text{MoS}_2$  for the anode materials is beneficial to lithium-ion batteries (LIBs). Wei *et al.*<sup>33</sup> studied the electrochemical reactions of  $\text{MoS}_2$  nanosheets in LIBs. Their study represented that intercalation of Li ions into  $\text{MoS}_2$  anode contributes the electrochemical charge storage. However, the low conductive of  $\text{MoS}_2$  and its aggregation during the electrode manufacturing process greatly hinder the development of LIBs.<sup>34,35</sup> In order to improve the performance of  $\text{MoS}_2$  as an electrode material for LIBs, there are two main options, one is to change the structure of  $\text{MoS}_2$  material, and the other is to prepare  $\text{MoS}_2$  composites.

On the one hand, Zhao *et al.*<sup>36</sup> studied  $\text{MoS}_2$  materials with nanotube structures to improve electrochemical performance. They reported a facile wet etching method for the preparation of low crystalline  $\text{MoS}_2$  nanotubes. First,  $\text{MoO}_3$  nanobelts ( $\text{MoO}_3$  NBs) were prepared by hydrothermal method. Sodium molybdate dihydrate ( $\text{Na}_2\text{MoO}_4 \cdot 2\text{H}_2\text{O}$ ) and nitric acid were used in this step. Second, 3D  $\text{MoS}_2$  nanomasks were grown *in situ* on  $\text{MoO}_3$  NBs, which was obtained by the chemical reaction of sublimed sulfur with  $\text{MoO}_3$  NBs in CVD quartz tube. Finally,

$\text{MoS}_2$  nanotubes ( $\text{MoS}_2$  NTs) were synthesized by mixing the previously obtained  $\text{MoO}_3/\text{MoS}_2$  NBs with concentrated hydrochloric acid. As demonstrated in Fig. 2a, the inner  $\text{MoO}_3$  are etched with concentrated hydrochloric acids to yield low crystalline  $\text{MoS}_2$  NTs. With the increase of etching times, the molybdenum oxide is gradually removed which allowed the internal cavity of  $\text{MoS}_2$  NTs to be emptied. After the fourth etching process, most of the molybdenum oxides were removed to give  $\text{MoS}_2$  NTs (Fig. 2b).

The electrochemical test results illustrated that  $\text{MoS}_2$  NTs, as the anode material for LIBs, reached a specific capacity of  $1253 \text{ mA g}^{-1}$  at a current rate of  $200 \text{ mA g}^{-1}$  and was stabilized after 250 cycles. Obviously, the low crystalline  $\text{MoS}_2$  NTs have even higher specific capacity and cyclic performance than the reported electrode materials.<sup>37,38</sup>

On the other hand, some researchers have investigated  $\text{MoS}_2$  nanocomposites to improve the electrochemical properties of  $\text{MoS}_2$  in LIBs.

Wu *et al.*<sup>34</sup> reported an electrode material of two-layer carbon-coated  $\text{MoS}_2$ /carbon nanofiber ( $\text{MoS}_2/\text{C/C}$  fiber) which prepared by hydrothermal and electrospinning method. First,  $\text{MoS}_2$  spheres were obtained by hydrothermal. Hexaammonium heptamolybdate tetrahydrate ( $(\text{NH}_4)_6\text{Mo}_7\text{O}_{24} \cdot 4\text{H}_2\text{O}$ ), thiourea ( $\text{NH}_2\text{CSNH}_2$ ), and polyvinylpyrrolidone (PVP) were used in this step. Second,  $\text{MoS}_2/\text{C}$  spheres were fabricated by using glucose and the above-obtained  $\text{MoS}_2$  spheres. Finally, they synthesized  $\text{MoS}_2/\text{C/C}$  nanofiber by electrospinning method. Polyacrylonitrile (PAN), *N,N*-dimethylformamide (DMF) and the above obtained  $\text{MoS}_2/\text{C}$  spheres were used. The preparation process of  $\text{MoS}_2/\text{C/C}$  fiber is shown in Fig. 2c.

Meanwhile, Zhang *et al.*<sup>35</sup> synthesized  $\text{TiO}_2/\text{C}/\text{MoS}_2$  microspheres as anodes for LIBs.  $\text{TiO}_2/\text{C}/\text{MoS}_2$  microspheres were prepared by solvent-thermal method and calcination. First of all they used PVP, acetic acid and tetrabutyltitanate (TBT) in a Teflon-lined autoclave for the reaction to prepare  $\text{TiO}_2/\text{C}$  materials. Secondly,  $\text{TiO}_2/\text{C}/\text{MoS}_2$  was synthesized by the obtained  $\text{TiO}_2/\text{C}$ , ammonium molybdatetetrahydrate ( $(\text{NH}_4)_6\text{Mo}_7\text{O}_{24} \cdot 4\text{H}_2\text{O}$ ) and thiourea ( $\text{CH}_4\text{N}_2\text{S}$ ). The preparation process of  $\text{TiO}_2/\text{C}/\text{MoS}_2$  microsphere is shown in Fig. 2e.

No matter  $\text{MoS}_2$  is compounded with carbon materials or  $\text{TiO}_2$  materials, the electrochemical properties of  $\text{MoS}_2$  materials have been improved. On the one hand, for the  $\text{MoS}_2/\text{C/C}$  electrode, the double-layer carbon coating (Fig. 2d) could not only suppress the irreversible reaction, but also confine the volume change during the lithiation/delithiation process.<sup>34</sup> Moreover,  $\text{MoS}_2/\text{C/C}$  fiber has better cycling performance than  $\text{MoS}_2$  spheres (Fig. 2g). On the other hand, the unique structure with flower-shaped of  $\text{TiO}_2/\text{C}/\text{MoS}_2$  (Fig. 2f) could not only enlarge the electrolyte-electrode interface area but also shorten the diffusion length of  $\text{Li}^+$  intercalation/deintercalation.<sup>35</sup> Compared with  $\text{MoS}_2$  materials, the cycling performance of  $\text{TiO}_2/\text{C}/\text{MoS}_2$  are enhanced (Fig. 2h).

### 2.2 Sodium-ion batteries

Sodium ion batteries (SIBs) are considered as an alternative to LIBs because of their abundant reserves and low cost. However,



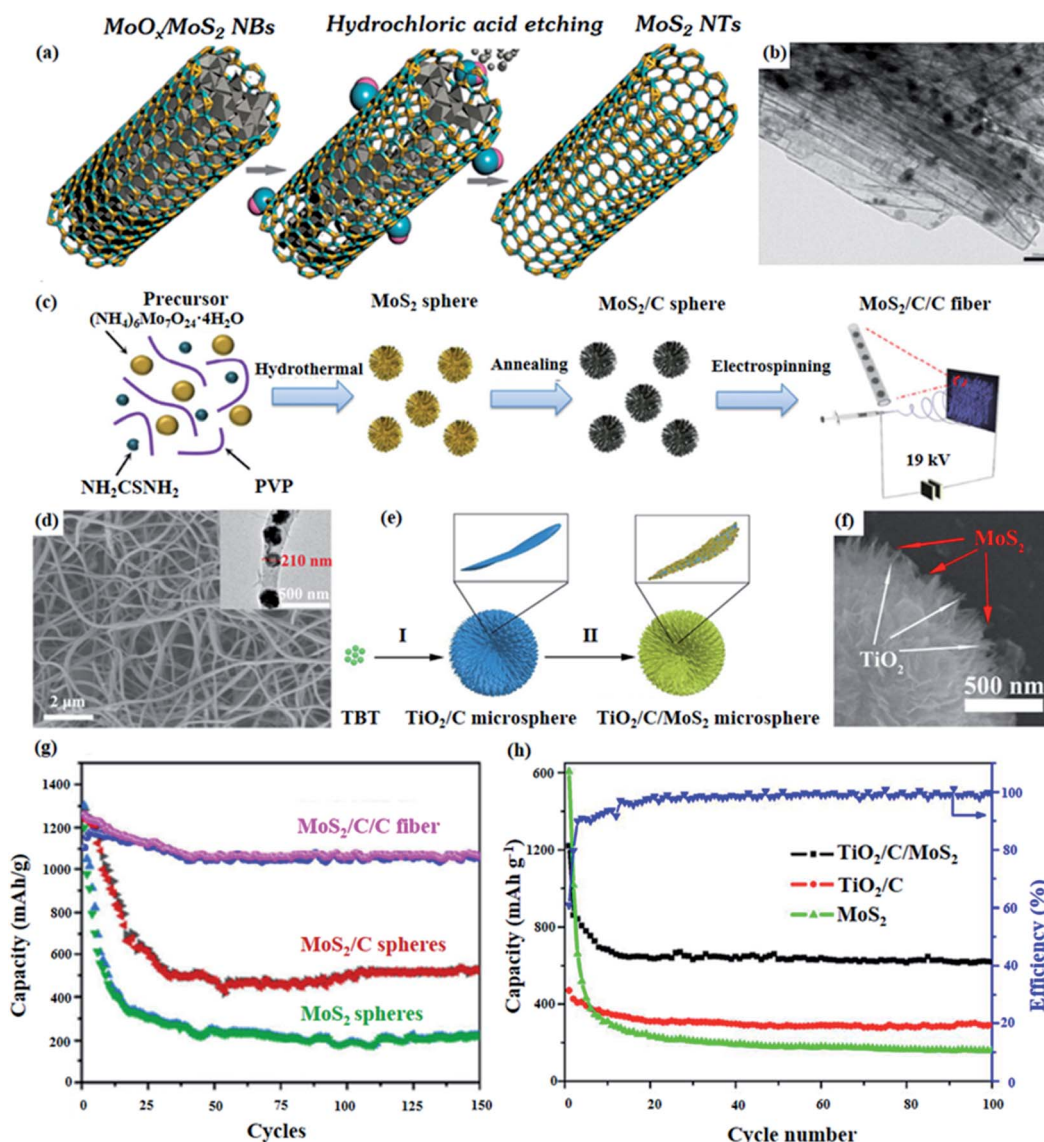


Fig. 2 (a)  $\text{MoS}_2$  NTs are obtained after etching  $\text{MoO}_x/\text{MoS}_2$  NBs with concentrated hydrochloric acid.<sup>36</sup> (b)  $\text{MoS}_2$  NTs obtained from the fourth etching.<sup>36</sup> (c) Schematic illustration of the preparation process of  $\text{MoS}_2/\text{C}/\text{C}$  fiber.<sup>34</sup> (d) SEM images of  $\text{MoS}_2/\text{C}/\text{C}$  fiber. The inset is a magnified TEM image of the sample.<sup>34</sup> (e) Schematic diagram of the synthesis of  $\text{TiO}_2/\text{C}/\text{MoS}_2$  microsphere.<sup>35</sup> (f) SEM images of  $\text{TiO}_2/\text{C}/\text{MoS}_2$  microsphere.<sup>35</sup> (g) Capacity retention of the  $\text{MoS}_2$ ,  $\text{MoS}_2/\text{C}$ , and  $\text{MoS}_2/\text{C}/\text{C}$  fiber electrodes at a current density of  $0.2 \text{ A g}^{-1}$  for the subsequent 150 cycles.<sup>36</sup> (h) Comparative cycling performance of  $\text{MoS}_2$ ,  $\text{TiO}_2/\text{C}$  and the  $\text{TiO}_2/\text{C}/\text{MoS}_2$  microsphere at a current density of  $100 \text{ mA g}^{-1}$ .<sup>35</sup>

$\text{Na}^+$  has larger radius than  $\text{Li}^+$ ,<sup>39</sup> which hinders the development of SIBs. As a highly promising electrode material,  $\text{MoS}_2$  has not only a layered structure but also a large interlayer spacing, which promises to solve the inherent defects of SIBs. However,  $\text{MoS}_2$  also has inherent limitations, such as low intrinsic electron conductivity. In response to these characteristics, some researchers have prepared composites of  $\text{MoS}_2$ <sup>40–43</sup> and others have improved the structure of  $\text{MoS}_2$  by doping or inserting molecules to achieve improved electrochemical properties.<sup>40–45</sup>

Pan *et al.*<sup>42</sup> reported a simple template method to prepared  $\text{MoS}_2/\text{amorphous carbon (C)}$  microtubes (MTs) composed of heterostructured  $\text{MoS}_2/\text{C}$  nanosheets. The synthesis of  $\text{MoS}_2/\text{C}$  MTs was achieved by a three-step procedure: first, obtaining  $\text{Sb}_2\text{S}_3$  microrods by a simple hydrothermal method, second,

$\text{MoS}_2/\text{C}$  nanosheets were grown on the outer surface of  $\text{Sb}_2\text{S}_3$  microrods by using sodium molybdate dehydrate ( $\text{Na}_2\text{MoO}_4 \cdot 2\text{H}_2\text{O}$ ),  $\text{N}_2\text{H}_4\text{CS}$ , and glucose ( $\text{C}_6\text{H}_{12}\text{O}_6$ ) in a Teflon-lined stainless steel autoclave for chemical reaction, and third,  $\text{MoS}_2/\text{C}$  MTs were obtained by removing  $\text{Sb}_2\text{S}_3$  microrods *via* annealing. The synthesis schematic is shown in Fig. 3a. Electrochemical measurements demonstrated that  $\text{MoS}_2/\text{C}$  MTs possessed high specific capacity and excellent stability, improving the electrochemical performance of SIBs.

Similarly, some researchers have also reported composites of  $\text{MoS}_2$  for enhancing the electrochemical performance of SIBs.

The  $\text{MoS}_2/\text{carbon nanofibers (MoS}_2/\text{CNFs)}$  were prepared by a two-step procedures: first, obtaining ammonium tetrathiomolybdate (AMT), and second, synthesizing  $\text{MoS}_2/\text{CNFs}$  by



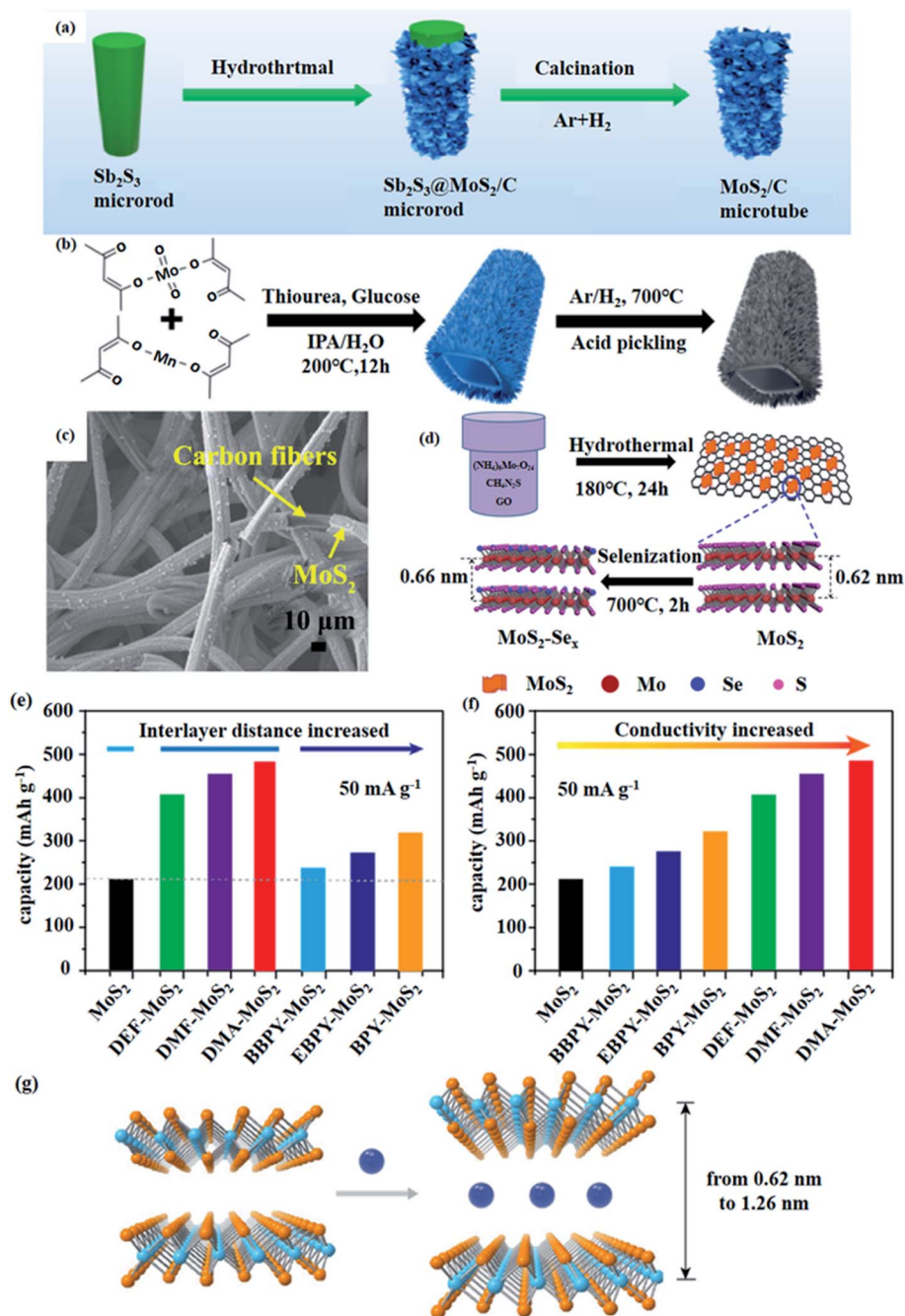


Fig. 3 (a) Schematic illustration of the synthesis process of  $\text{MoS}_2/\text{C}$  MTs.<sup>42</sup> (b) Schematic diagram of the fabrication process of  $\text{MoS}_2/\text{C}$  hollow rhomboids.<sup>41</sup> (c) FESEM images of OMSCF calcined in air at  $400^\circ\text{C}$  (OMSCF-400).<sup>43</sup> (d) Schematic illustration of the synthesis of  $\text{MoS}_2/\text{C}$  hollow rhomboids.<sup>41</sup> (e) Capacity of all intercalated  $\text{MoS}_2$  at  $50\text{ mA g}^{-1}$  arranged according to the interlayer distance, respectively.<sup>44</sup> (f) Capacity of all intercalated  $\text{MoS}_2$  at  $50\text{ mA g}^{-1}$  arranged according to conductivity, respectively.<sup>44</sup> (g) Schematic of intercalation of molecules into  $\text{MoS}_2$ .<sup>44</sup>

electrospinning and high temperature carbonization.  $\text{MoS}_2/\text{CNFs}$  have a large specific surface area and high electrical conductivity, which enhances Na storage performance.<sup>40</sup>

The  $\text{MoS}_2/\text{C}$  hollow rhomboids (MCHRs) were fabricated by a sample one-pot solvothermal reaction (Fig. 3b). First of all, manganese(II)acetylacetonate ( $\text{Mn}(\text{acac})_2$ ), molybdenyl acetylacetonate ( $\text{MoO}_2(\text{acac})_2$ ) were dispersed in distilled water and isopropanol. And then, glucose and thiourea were incorporated

into the mixture. Finally, the mixture was annealed after reaction in a Teflon-lined autoclave and washed several times with dilute hydrochloric acid and deionized water to obtain MCHRs. Electrochemical measurements revealed that MCHRs had better Na storage performance, higher rate capability, more stable cycling performance and superior reversible specific capacity.<sup>41</sup>

The vertically oxygen-incorporated MoS<sub>2</sub> nanosheets coated on carbon fiber (OMSCF) were synthesized by hydrothermal process and calcination reaction in air. First, carbon fiber was extracted from commercial wet tissue (Vinda Paper Group) with concentrated hydrochloric acid. Second, graphite oxide (GO) was synthesized through the modified Hummers' method. Finally, MoS<sub>2</sub>/carbon fibers (MSCF) were obtained by hydrothermal method. The FESEM images of OMSCF are shown in Fig. 3c. Oxygen atoms are incorporated into MoS<sub>2</sub> by the MSCF calcined in air. The incorporation of oxygen not only creates more defects, but also expands the interlayer spacing. The composite of carbon fiber and MoS<sub>2</sub> nanosheets not only

improves electronic conductivity, but also enhances structural stability.<sup>43</sup>

In addition, Zhang *et al.*<sup>45</sup> prepared ternary MoS<sub>2-x</sub>Se<sub>x</sub> alloy/graphene (MoS<sub>2-x</sub>Se<sub>x</sub>/G) composite through hydrothermal reaction and selenization treatment (Fig. 3d). The interlayer spacing of MoS<sub>2</sub> is expanded due to the doping of Se atoms which facilitates Na<sup>+</sup> fast transfer. Meanwhile, the electronic conductivity of composite is enhanced due to graphene, which boosts the electrochemical performance for NIBs.

Dai *et al.*<sup>44</sup> reported a series of molecule-intercalated MoS<sub>2</sub> as anode materials for SIBs. The molecular intercalation method expands the interlayer spacing as well as increases the electrical

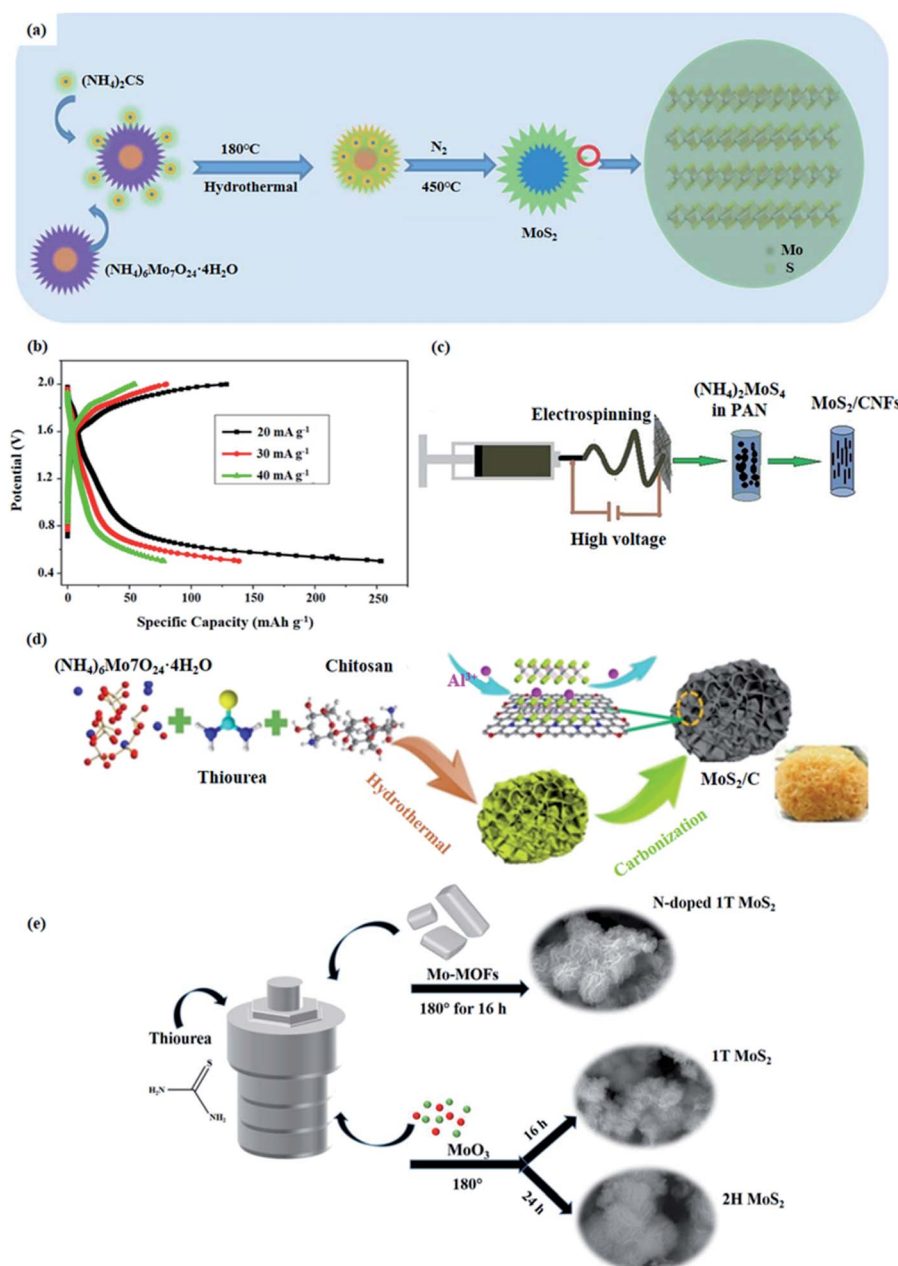


Fig. 4 (a) Schematic illustration of MoS<sub>2</sub> microspheres prepared by hydrothermal method.<sup>47</sup> (b) The first discharge-charge curves at different current densities.<sup>47</sup> (c) Schematic illustration of the preparation process of MoS<sub>2</sub>/CNFs.<sup>48</sup> (d) The preparation process of MNC.<sup>49</sup> (e) The synthesis of N-doped 1T MoS<sub>2</sub>, pure 1T MoS<sub>2</sub>, and 2H MoS<sub>2</sub>.<sup>50</sup>



conductivity of MoS<sub>2</sub> (Fig. 3e and f). The interlayer spacing can be varied in the range of 0.62 to 1.26 nm precisely by inserting different molecules (Fig. 3g).

In the example of the dimethylacetamide–MoS<sub>2</sub> (DAM–MoS<sub>2</sub>) construct, MoS<sub>2</sub> was synthesized by hydrothermal method firstly. Second, squeezing small DAM molecules into the layers.<sup>46</sup> Specifically, DAM, (NH<sub>4</sub>)<sub>6</sub>Mo<sub>7</sub>O<sub>24</sub>·4H<sub>2</sub>O, Na<sub>2</sub>S·9H<sub>2</sub>O, N<sub>2</sub>H<sub>4</sub>·H<sub>2</sub>O and deionized water were mixed. Then, the mixture was placed in Teflon-liner autoclave and heated at 230 °C for 24 h. Finally, dark powders were collected after naturally cooled to RT. Benefiting from the expanded interlayer spacing and improved conductivity, the electrochemical performance of SIBs with MoS<sub>2</sub> as the electrode material has been enhanced.

### 2.3 Other rechargeable batteries

Aluminum ion batteries (AIBs) are also members of energy storage systems. MoS<sub>2</sub> and its composites can be used as cathode materials for AIBs. Li *et al.*<sup>47</sup> prepared MoS<sub>2</sub> microspheres structure by hydrothermal method. The preparation process is shown in the Fig. 4a. First, the MoS<sub>2</sub> microsphere precursor was synthesized by using (NH<sub>4</sub>)<sub>6</sub>Mo<sub>7</sub>O<sub>24</sub>·4H<sub>2</sub>O and (NH<sub>4</sub>)<sub>2</sub>CS in a hydrothermal method. And then, MoS<sub>2</sub> microsphere was obtained by heat treatment in a nitrogen atmosphere.

Fig. 4b depicts the electrochemical performance of MoS<sub>2</sub> microspheres. Obviously, the electrochemical performance of AIBs with MoS<sub>2</sub> microsphere cathode material is not excellent. The reason for this can be attributed to the inherent defects of MoS<sub>2</sub>. Therefore, future research focusing on enhancing the electrochemical properties of MoS<sub>2</sub> electrode materials is needed.

Yang *et al.*<sup>48</sup> reported a flexible free-standing MoS<sub>2</sub>/CNFs cathode for rechargeable AIBs. As shown in Fig. 4c, the MoS<sub>2</sub>/CNFs are prepared by electrospinning and annealing treatment. As electrode materials for AIBs, MoS<sub>2</sub>/CNFs exhibit better cycling stability and higher rate capacity than MoS<sub>2</sub> microspheres.

In order to overcome the defects of MoS<sub>2</sub> and achieve the improved electrochemical performance of AIBs, another method is to use N-doped carbon materials compounded with MoS<sub>2</sub> as a cathode material for AIBs. Guo *et al.*<sup>49</sup> synthesized interlayer-expanded MoS<sub>2</sub>/N-doped carbon (MNC) with a three-dimensional (3D) hierarchical structure by a hydrothermal method and calcination. Fig. 4d represents the synthesis of MNC. Electrochemical test results illustrated that MNC had excellent cycling ability and high discharge capacity, which were owing to the unique 3D structure provides a large specific surface area and the N-doped carbon expands the interlayer spacing of MoS<sub>2</sub>.

Aqueous zinc ion batteries (ZIBs) are one of the rechargeable batteries based on divalent cations. Nevertheless, Zn<sup>2+</sup> has strong interactions with water molecules, increasing the difficulty of Zn<sup>2+</sup> diffusion and intercalation,<sup>54</sup> which hinders the development of ZIBs. To address these problems, researchers used MoS<sub>2</sub> as an electrode material to improve the electrochemical performance of ZIBs by increasing its interlayer spacing through doping with nitrogen or oxygen.<sup>50,54</sup>

In the example of the N-doped MoS<sub>2</sub>, Mo–organic framework (Mo–MOF) served as the nitrogen source. Basing on the one-step hydrothermal sulfurization, N-doped MoS<sub>2</sub> was prepared.<sup>50</sup> Ideally, the 1T and 2H phases of MoS<sub>2</sub> can be obtained by different reaction conditions (Fig. 4e).

The electrochemical test results illustrated that N-doped 1T MoS<sub>2</sub> has not only high multiplicative performance but also superior cycling stability, which greatly improves the electrochemical performance of ZIBs.

In order to better display the synthesis and application of MoS<sub>2</sub>-based nanomaterials in electrode materials, the preparation methods and batteries performance are summarized in Table 1. In addition, we also collected some typical nanomaterials for battery applications to compare with MoS<sub>2</sub>.<sup>51–53</sup>

## 3. Applications and synthesis strategies of MoS<sub>2</sub> in catalyst for water splitting

The use of large amounts of fossil fuels has led to increasing environmental degradation, therefore, it is essential to produce clean, renewable energy. Hydrogen energy, as one of the clean energy sources, has been widely researched in recent years. Electrocatalytic water splitting and photocatalytic water splitting are recognized as efficient methods for the preparation of hydrogen.<sup>55–60</sup> The water splitting reaction requires an efficient catalyst. It is well known that MoS<sub>2</sub> is a lamellar structure with abundant active sites at the edges. This property makes it a promising non-precious metal catalyst with large numbers of applications in catalysis. However, the defects of MoS<sub>2</sub> with low bulk conductivity and anisotropic electrical transport restrict the catalytic efficiency. Therefore, researchers have developed amount of MoS<sub>2</sub> composite catalysts to improve the catalytic efficiency.

### 3.1 Electrocatalyst

According to previous reports, either 1T-phase MoS<sub>2</sub> catalysts or MoS<sub>2</sub> composites catalysts have efficient catalytic performance in the HER. In detail, 1T-phase MoS<sub>2</sub> has higher catalytic performance than 2H-phase MoS<sub>2</sub>, benefiting from the fast charge transfer rate in the metal phase.<sup>61</sup> The compounding of MoS<sub>2</sub> with MoN can not only improve the electrical conductivity of MoS<sub>2</sub>, but also make MoS<sub>2</sub> have good stability in acidic and alkaline environments.<sup>62</sup> The compounding of MoS<sub>2</sub> with CNFs can improve the electrical conductivity of MoS<sub>2</sub> and restrict the growth of MoS<sub>2</sub> nanosheets.<sup>63</sup> In addition, MoS<sub>2</sub> composites can be used as bifunctional and efficient electrocatalysts for water splitting. For example, CoS<sub>2</sub>–C@MoS<sub>2</sub> exhibits both excellent HER catalytic performance and good oxygen evolution reaction (OER) catalytic performance.<sup>64</sup> MoS<sub>2</sub> compounded with Mo<sub>2</sub>N-containing multichannel hollow CNFs (Mo<sub>2</sub>N–MoS<sub>2</sub> MCNFs) also possesses excellent HER and OER catalytic properties.<sup>65</sup> Subsequently, the preparation of these materials will be described.

1T-MoS<sub>2</sub> was synthesized by hydrothermal reaction. Specifically, (NH<sub>4</sub>)<sub>6</sub>Mo<sub>7</sub>O<sub>24</sub>·4H<sub>2</sub>O and N<sub>2</sub>H<sub>4</sub>CS were dissolved in



**Table 1** MoS<sub>2</sub>-based nanocomposites for electrode materials

| No. | Materials  | Preparation  | Mo source  | S source   | Morphology of MoS <sub>2</sub>           | Battery electrodes   | Specific capacity (mA h g <sup>-1</sup> ) | Cycling number | Current rate (mA g <sup>-1</sup> ) | Ref. |
|-----|--|--|--|--|--|--|---|----------------|------------------------------------|------|
| 1   | MoS <sub>2</sub>                                     | Wet etching method                                 | Na <sub>2</sub> MoO <sub>4</sub> ·2H <sub>2</sub> O                                | Sulfur   | Nanotube                                 | LIBs cathode   | 1150                                      | 250            | 200                                | 36   |
| 2   | MoS <sub>2</sub> /C/C                                | Hydrothermal and electrospinning method            | (NH <sub>4</sub> ) <sub>6</sub> Mo <sub>7</sub> O <sub>24</sub> ·4H <sub>2</sub> O | N <sub>2</sub> H <sub>4</sub> CS                 | Sphere                                   | LIBs anode   | 1062                                      | 150            | 200                                | 34   |
| 3   | TiO <sub>2</sub> /C/MoS <sub>2</sub>                 | Solvent-thermal method and calcination             | (NH <sub>4</sub> ) <sub>6</sub> Mo <sub>7</sub> O <sub>24</sub> ·4H <sub>2</sub> O | N <sub>2</sub> H <sub>4</sub> CS                 | Fish-scale-shaped (10 nm in size)        | LIBs anode   | 621                                       | 100            | 100                                | 35   |
| 4   | MoS <sub>2</sub> /C                                  | Template method                                    | Na <sub>2</sub> MoO <sub>4</sub> ·2H <sub>2</sub> O                                | N <sub>2</sub> H <sub>4</sub> Cs                 | Nanosheet                                | SIBs anode   | 484.9                                     | 1500           | 2000                               | 42   |
| 5   | MoS <sub>2</sub> /CNFs                               | Electrospinning and high temperature carbonization | AMT  | AMT  | Single-layer structure                   | SIBs anode   | 485                                       | 100            | 100                                | 40   |
| 6   | MCHRs  | One-pot solvothermal reaction                      | MoO <sub>2</sub> (acac) <sub>2</sub>   | N <sub>2</sub> H <sub>4</sub> CS                 | Nanosheet                                | SIBs anode   | 265                                       | 3000           | 10 000                             | 41   |
| 7   | OMSCF  | Hydrothermal process and calcination               | Na <sub>2</sub> MoO <sub>4</sub>   | N <sub>2</sub> H <sub>4</sub> CS                 | Nanosheet                                | SIBs anode   | 330                                       | 100            | 100                                | 43   |
| 8   | MoS <sub>2</sub> -xSe <sub>x</sub> /G                | Hydrothermal reaction and selenization treatment   | (NH <sub>4</sub> ) <sub>6</sub> Mo <sub>7</sub> O <sub>24</sub> ·4H <sub>2</sub> O | N <sub>2</sub> H <sub>4</sub> CS                 | —  | SIBs anode   | 178                                       | 700            | 2000                               | 45   |
| 9   | DAM-MoS <sub>2</sub>                                 | Hydrothermal method                                | (NH <sub>4</sub> ) <sub>6</sub> Mo <sub>7</sub> O <sub>24</sub> ·4H <sub>2</sub> O | Na <sub>2</sub> S·9H <sub>2</sub> O              | Layered structure (0.62–1.24 nm in size) | SIBs anode   | 420                                       | 600            | 100                                | 44   |
| 10  | MoS <sub>2</sub>                                     | Hydrothermal method                                | (NH <sub>4</sub> ) <sub>6</sub> Mo <sub>7</sub> O <sub>24</sub> ·4H <sub>2</sub> O | N <sub>2</sub> H <sub>4</sub> CS                 | Microsphere                              | AIBs cathode   | 66.7                                      | 100            | 40                                 | 47   |
| 11  | MoS <sub>2</sub> /CNFs                               | Electrospinning and annealing treatment            | (NH <sub>4</sub> ) <sub>2</sub> MoS <sub>4</sub>                                   | (NH <sub>4</sub> ) <sub>2</sub> MoS <sub>4</sub> | Nanosheet                                | AIBs cathode   | 130                                       | 200            | 100                                | 48   |
| 12  | MNC  | Hydrothermal method and calcination                | (NH <sub>4</sub> ) <sub>6</sub> Mo <sub>7</sub> O <sub>24</sub> ·4H <sub>2</sub> O | N <sub>2</sub> H <sub>4</sub> CS                 | Nanosheet                                | AIBs cathode   | 127.5                                     | 1700           | 1000                               | 49   |
| 13  | N-doped MoS <sub>2</sub>                             | One-step hydrothermal sulfurization                | MO-MOF   | N <sub>2</sub> H <sub>4</sub> CS                 | Nanoflower                               | ZIBs cathode   | 98.1                                      | 1000           | 3000                               | 50   |
| 14  | hBN/C  | Liquid-phase shear exfoliation method              | —  | —  | —  | LIBs separators  | 158                                       | 100            | —                                  | 51   |
| 15  | rGO/Al   | Electrospinning                                    | —  | —  | —  | LiNi <sub>0.5</sub> Mn <sub>1.5</sub> O <sub>4</sub> cathode | 109.5                                     | 840            | —                                  | 52   |
| 16  | P <sub>4</sub> Nb <sub>2</sub> O <sub>15</sub> @CNTs | Solvothermal method                                | —  | —  | —  | LIBs anode   | 250                                       | 500            | —                                  | 53   |



distilled water to form a homogeneous solution, and then the solution was put into a Teflon-lined stainless steel autoclave for reaction. The formation of 1T phase or 2H phase depends on the reaction temperature.

Hierarchical  $\text{MoS}_2/\text{MoN}$  heterostructures were obtained by a simple hydrothermal reaction and nitridation treatment.  $\text{MoS}_2$  nanospheres were synthesized from  $\text{N}_2\text{H}_4\text{CS}$  and hexaammonium molybdate in a hydrothermal reaction. Subsequently, the layered  $\text{MoS}_2/\text{MoN}$  heterostructures were synthesized by nitriding under ammonia atmosphere.

$\text{MoS}_2$ -carbon CNFs were prepared by electrospinning and graphitization treatment. First,  $(\text{NH}_4)_2\text{MoS}_4$  was dissolved in PAN solution and used for electrospinning to prepare PAN/

$(\text{NH}_4)_2\text{MoS}_4$  (PANAMo) nanofibers. Afterwards, the precursor nanofibers were graphitized to obtain  $\text{MoS}_2$ -CNFs hybrids.

$\text{CoS}_2$ -C@ $\text{MoS}_2$  core-shell nanofibers were fabricated by electrospinning method, carbonization treatment and hydrothermal synthesis. First, a certain amount of PAN and  $\text{Co}(\text{Ac})_2 \cdot 4\text{H}_2\text{O}$  were dissolved in DMF to prepare  $\text{Co}(\text{Ac})_2/\text{PAN}$  membranes by electrospinning method. Later, the Co-C nanofibers were obtained by carbonization under Ar atmosphere. Second,  $\text{CoS}_2$ -C@ $\text{MoS}_2$  core-shell nanofibers were prepared by a simple hydrothermal method using  $(\text{NH}_4)_2\text{MoS}_4$  as the S source.

As depicted in Fig. 5a, the synthesis of  $\text{Mo}_2\text{N}$ - $\text{MoS}_2$  MCNFs was achieved by a four-step procedure. First, a certain amount

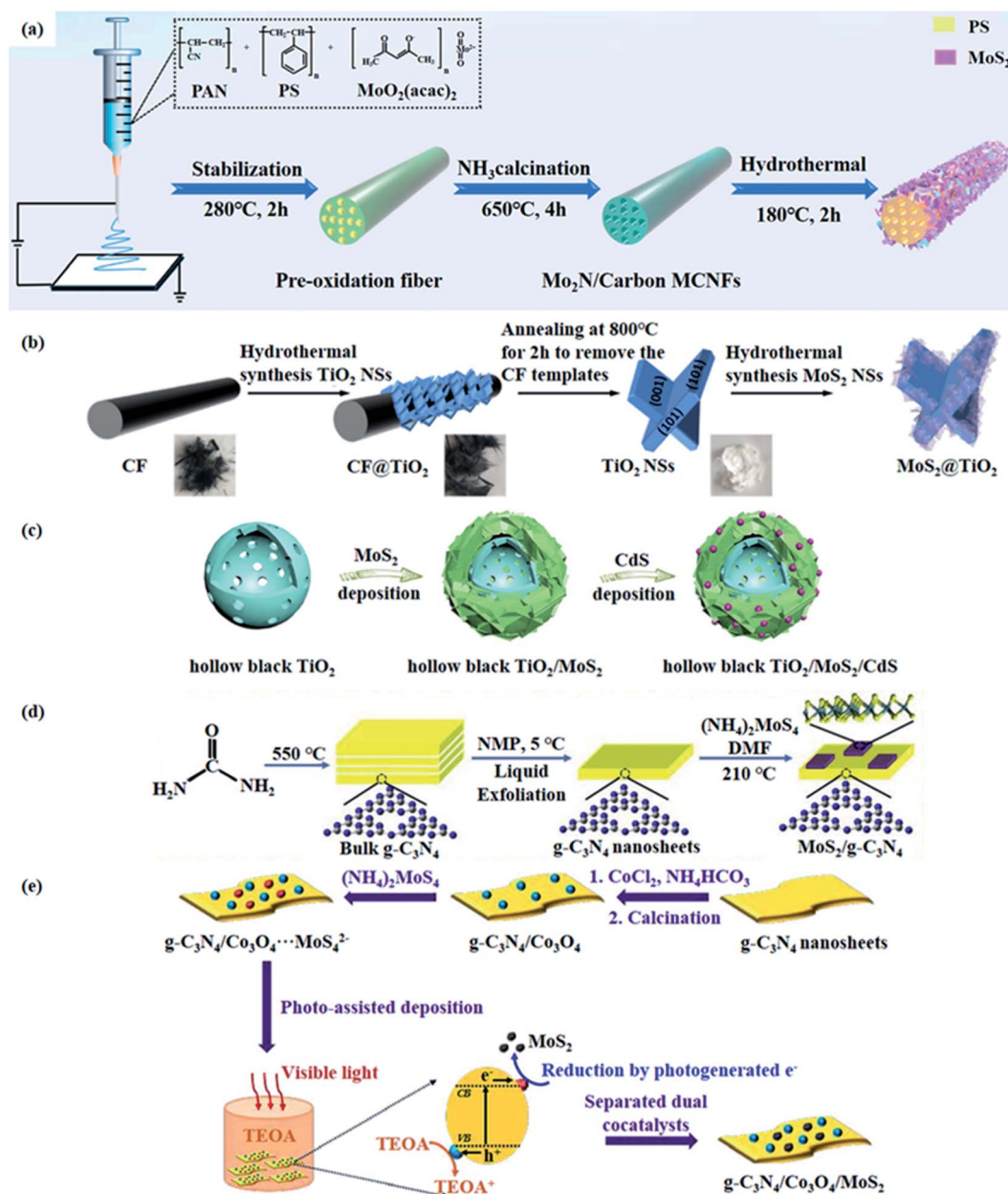


Fig. 5 The diagrammatic sketch for the preparation of (a)  $\text{Mo}_2\text{N}$ - $\text{MoS}_2$  MCNFs,<sup>65</sup> (b)  $\text{MoS}_2$ @ $\text{TiO}_2$  composites,<sup>68</sup> (c)  $\text{TiO}_2$ /MoS<sub>2</sub>/CdS tandem heterojunction,<sup>69</sup> (d) 2D-2D  $\text{MoS}_2$ /g- $\text{C}_3\text{N}_4$  composites<sup>70</sup> and (e) g- $\text{C}_3\text{N}_4$ /Co<sub>3</sub>O<sub>4</sub>/MoS<sub>2</sub> heterojunction.<sup>71</sup>



Table 2 MoS<sub>2</sub>-based nanocomposites for electrocatalyst and photocatalyst

| No. | Materials                                | Preparation  | Mo source  | S source   | Morphology of MoS <sub>2</sub> | Electrocatalyst  |   | Ref. |
|-----|--|--|--|--|--------------------------------|--|---|------|
|     |  |  |  |  |                                | Tafel slope (mV dec <sup>-1</sup> )                      | Overpotential (mV vs. RHE) at <i>J</i> = 10 mA cm <sup>-2</sup> |      |
| 1   | 1T-MoS <sub>2</sub>                      | Hydrothermal reaction  | (NH <sub>4</sub> ) <sub>6</sub> Mo <sub>7</sub> O <sub>24</sub> ·4H <sub>2</sub> O | Thiourea   | Nanosheet                      | 54 (HER)   | 214 (HER)   | 61   |
| 2   | MoS <sub>2</sub> /MoN                    | Hydrothermal reaction and nitridation treatment                                | Hexaammonium molybdate   | Thiourea   | Nanosphere                     | 98 (HER, KOH); 87 (HER, H <sub>2</sub> SO <sub>4</sub> ) | 132 (HER, KOH); 117 (HER, H <sub>2</sub> SO <sub>4</sub> )      | 62   |
| 3   | MoS <sub>2</sub> /CNFs                   | Electrospinning and graphitization treatment                                   | (NH <sub>4</sub> ) <sub>2</sub> MoS <sub>4</sub>                                   | (NH <sub>4</sub> ) <sub>2</sub> MoS <sub>4</sub> | Nanoplate                      | 42 (HER)   | 93 (HER)  | 63   |
| 4   | CoS <sub>2</sub> -C@MoS <sub>2</sub>     | Electrospinning method, carbonization treatment and hydrothermal synthesis     | (NH <sub>4</sub> ) <sub>2</sub> MoS <sub>4</sub>                                   | (NH <sub>4</sub> ) <sub>2</sub> MoS <sub>4</sub> | Nanosheet                      | 61 (HER); 46 (OER)                                       | 173 (HER); 391 (OER)  | 64   |
| 5   | Mo <sub>2</sub> N-MoS <sub>2</sub> MCNFs | Electrospinning method, NH <sub>3</sub> calcination and hydrothermal synthesis | (NH <sub>4</sub> ) <sub>6</sub> Mo <sub>7</sub> O <sub>24</sub> ·4H <sub>2</sub> O | Thiourea   | Nanosheet                      | 68.9 (HER); 57.2 (OER)                                   | 131 (HER); 270 (OER)  | 65   |
| 6   | Graphene-hBN                             | Exfoliation and Hummer's method  | —  | —  | —                              | —  | 390 (HER)   | 66   |
| 7   | Cobalt- and nitrogen-codoped graphene    | Annealing strategy   | —  | —  | —                              | 73 (OER)   | 210 (OER)   | 67   |

| No. | Materials   | Preparation  | Mo source  | S source   | Morphology of MoS <sub>2</sub> | Photocatalyst   |   | Ref. |
|-----|---|--|--|--|--------------------------------|---|---|------|
|     |   |  |  |  |                                | H <sub>2</sub> evolution rate (mmol h <sup>-1</sup> g <sup>-1</sup> ) | H <sub>2</sub> evolution rate (mmol h <sup>-1</sup> g <sup>-1</sup> ) |      |
| 8   | MoS <sub>2</sub> @TiO <sub>2</sub>  | Hydrothermal/annealing treatment and subsequent photoreduction method                                | (NH <sub>4</sub> ) <sub>2</sub> MoS <sub>4</sub> | (NH <sub>4</sub> ) <sub>2</sub> MoS <sub>4</sub> | Nanosheet                      | 2.16  | —   | 68   |
| 9   | TiO <sub>2</sub> /MoS <sub>2</sub> /CdS   | Template-free solvothermal approach, solvothermal approach and wet chemical method                   | MoO <sub>3</sub>                                 | Thiourea   | Nanosheet                      | 9   | —   | 69   |
| 10  | MoS <sub>2</sub> /g-C <sub>3</sub> N <sub>4</sub>                                 | Direct heating of urea and a solvent-thermal method  | (NH <sub>4</sub> ) <sub>2</sub> MoS <sub>4</sub> | (NH <sub>4</sub> ) <sub>2</sub> MoS <sub>4</sub> | Nanosheet                      | 1.155   | —   | 70   |
| 11  | g-C <sub>3</sub> N <sub>4</sub> /Co <sub>3</sub> O <sub>4</sub> /MoS <sub>2</sub> | Two-step thermal treatment, coprecipitation-calcination strategy and <i>in situ</i> photo-deposition | (NH <sub>4</sub> ) <sub>2</sub> MoS <sub>4</sub> | (NH <sub>4</sub> ) <sub>2</sub> MoS <sub>4</sub> | MoS <sub>2</sub> nanocrystal   | 5.25  | —   | 71   |
| 12  | Sulfur-doped h-BN   | CVD  | —  | —  | —                              | 1.3485  | —   | 72   |

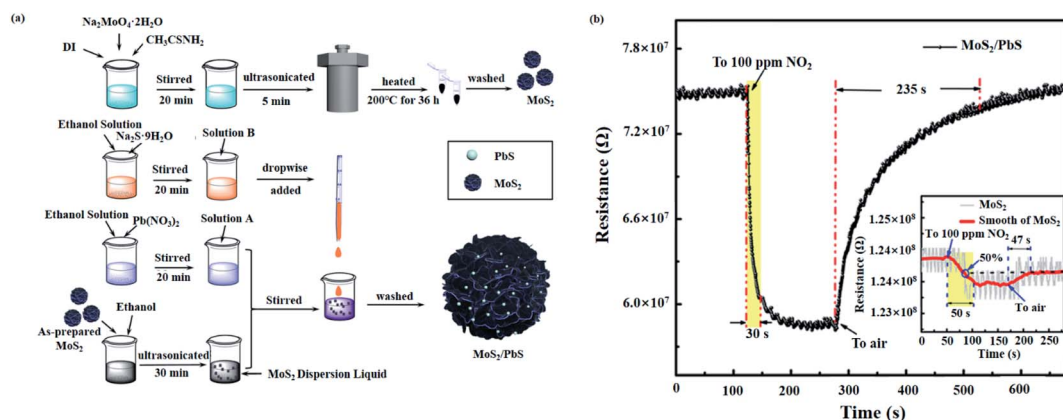


Fig. 6 (a) Preparation process of  $\text{MoS}_2/\text{PbS}$  composites.<sup>78</sup> (b) Transient response characteristic of  $\text{MoS}_2/\text{PbS}$  gas sensor at 100 ppm  $\text{NO}_2$ .<sup>78</sup>

of PAN and polystyrene (PS) were dissolved in DMF, stirred well and then  $\text{MoO}_2(\text{acac})_2$  was added to form a precursor solution for electrospinning to obtain  $\text{MoO}_2(\text{acac})_2@ \text{PAN/PS}$  fiber. Second, previously obtained fiber was pre-oxidized in air. Third,

$\text{Mo}_2\text{N/C}$  MCFs were prepared by calcination of the pre-oxidation fiber under  $\text{NH}_3$  atmosphere. During calcination, PS gradually decomposed, leading to the formation of channels in the fibers. Finally,  $\text{Mo}_2\text{N}-\text{MoS}_2$  MCNFs were successfully prepared by

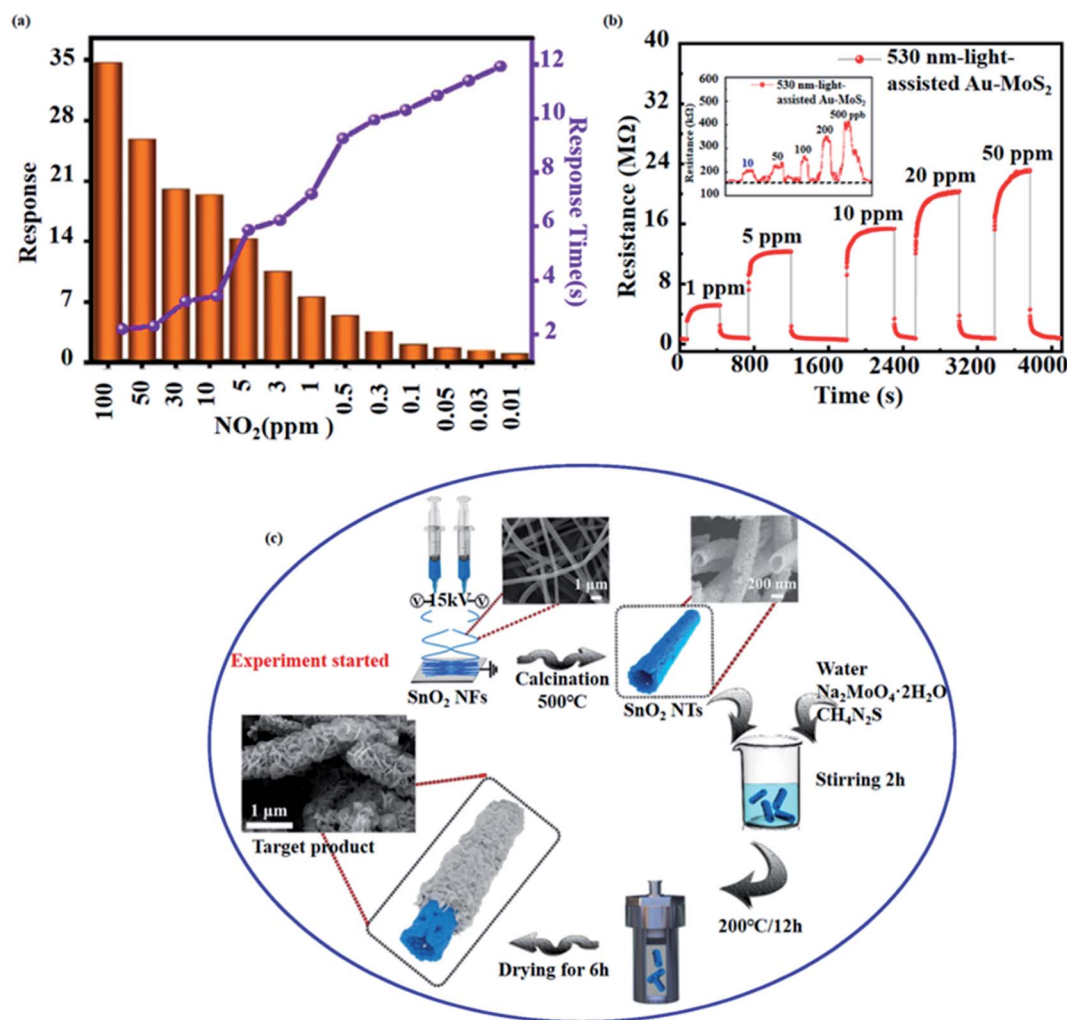


Fig. 7 (a) Response and response time of  $\text{MoS}_2@ \text{SnO}_2$  sensor to 0.01–100 ppm  $\text{NO}_2$ .<sup>79</sup> (b) Real-time sensing response curves of the 530 nm-light-assisted  $\text{Au}-\text{MoS}_2$  sensor at 1–50 ppm  $\text{NO}_2$ .<sup>80</sup> (c) Schematic diagram of the synthesis of  $\text{MoS}_2@ \text{SnO}_2$ .<sup>79</sup>

hydrothermal method to grow MoS<sub>2</sub> nanosheets on the surface of Mo<sub>2</sub>N/Carbon MCNFs.

### 3.2 Photocatalyst

Photocatalytic water splitting reaction is considered as one of the effective ways to prepare green, renewable energy, due to its ability to convert solar energy into hydrogen energy. In recent years, with the development of hydrogen preparation reaction by photocatalytic water splitting, more and more photocatalysts have been studied and prepared, including those prepared with graphite carbon nitride (g-C<sub>3</sub>N<sub>4</sub>), TiO<sub>2</sub> or CdS as materials. It has been shown that the compound of MoS<sub>2</sub> with the above materials can improve the catalytic activity of the photocatalyst and promote the preparation of hydrogen by water splitting.<sup>68–71,73</sup>

Hu *et al.*<sup>68</sup> prepared MoS<sub>2</sub>@TiO<sub>2</sub> composites by using combination of hydrothermal/annealing treatment with subsequent photoreduction method. It is noted that MoS<sub>2</sub> nanosheets can be selectively deposited on the (101) facets of TiO<sub>2</sub>, allowing for increased photocatalytic hydrogen production activity of the MoS<sub>2</sub>@TiO<sub>2</sub> composites. Sun *et al.*<sup>69</sup> fabricated a hollow TiO<sub>2</sub>/MoS<sub>2</sub>/CdS tandem heterojunction *via* three main steps. First, the hollow mesoporous TiO<sub>2</sub> spheres were synthesized by a template-free solvothermal approach. Second, MoS<sub>2</sub> nanosheets were coated on the surface of TiO<sub>2</sub> by a solvothermal approach. Finally, CdS nanoparticles were selectively deposited on the edges of MoS<sub>2</sub>

nanosheets through a wet chemical method. MoS<sub>2</sub> not only serves as an excellent cocatalyst, but also promotes charge separation and effectively inhibits the complexation of photogenerated electrons and holes. Yuan *et al.*<sup>70</sup> obtained 2D–2D MoS<sub>2</sub>/g-C<sub>3</sub>N<sub>4</sub> photocatalyst through a simple probe sonication assisted liquid exfoliation method and a solvent-thermal method. The large surface area of g-C<sub>3</sub>N<sub>4</sub> nanosheets and the large 2D nanointerface between MoS<sub>2</sub> and g-C<sub>3</sub>N<sub>4</sub> nanosheets greatly enhance the catalytic hydrogen production activity of the photocatalyst. Zhao *et al.*<sup>71</sup> synthesized g-C<sub>3</sub>N<sub>4</sub>/Co<sub>3</sub>O<sub>4</sub>/MoS<sub>2</sub> heterojunction *via* chemical deposition and photo-deposition method. Co<sub>3</sub>O<sub>4</sub> and MoS<sub>2</sub> were used as co-catalysts with efficient photocatalytic activity under visible light irradiation. Their synthesis schematic is demonstrated in Fig. 5b–e.

In order to better display the synthesis and application of MoS<sub>2</sub>-based nanomaterials in catalysis, the preparation methods and catalytic performance are summarized in Table 2. Furthermore, for comparison, we summarize performance parameters of some typical nanomaterials in electrocatalysis and photocatalysis at the end of the table.<sup>66,67,72</sup>

## 4. Applications and synthesis strategies of MoS<sub>2</sub> in gas sensors

Important factors affecting the performance of gas sensors have been reported to include specific surface area, semiconductor properties, and redox reaction active sites.<sup>74</sup> As mentioned

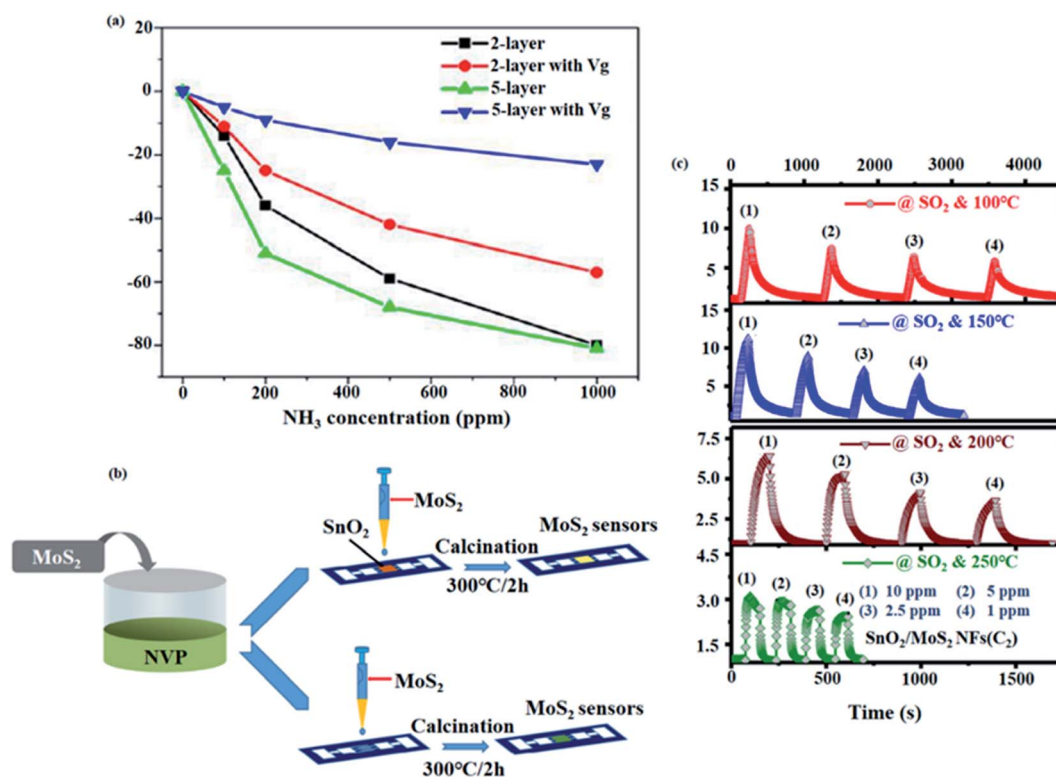


Fig. 8 (a) Sensitivity of 2-layer and 5-layer MoS<sub>2</sub> as a function of NH<sub>3</sub> concentration.<sup>74</sup> (b) Schematic diagram of the fabrication of MoS<sub>2</sub> sensors and MoS<sub>2</sub>/SnO<sub>2</sub> sensors.<sup>81</sup> (c) Response of MoS<sub>2</sub>/SnO<sub>2</sub> sensors to different concentrations of SO<sub>2</sub> gas at different operating temperatures.<sup>81</sup>



earlier, MoS<sub>2</sub> is a graphene-like material possessing a 2D layer structure with a large specific surface area and excellent semiconductor properties. In addition, it has been pointed out that MoS<sub>2</sub> has different affinities for different molecules,<sup>75</sup> which makes MoS<sub>2</sub> one of the promising materials for the preparation of gas sensors.

#### 4.1 MoS<sub>2</sub>-based gas sensors toward nitrogen dioxide

Nitrogen dioxide (NO<sub>2</sub>) is one of the prevalent pollutants in the air, as well as a toxic gas that endangers human health, causing great damage to human eyes and respiratory tracts even when exposed to concentrations as low as 3 ppm.<sup>76</sup> Therefore, it is urgent to develop gas sensors that can detect NO<sub>2</sub> effectively and rapidly. The detection of NO<sub>2</sub> by pure MoS<sub>2</sub> or MoS<sub>2</sub> composites as gas-sensitive elements is one of the main focuses of gas sensors research in recent years.

Using pure MoS<sub>2</sub> as gas sensitive element, some researches have prepared MoS<sub>2</sub> by chemical vapor deposition (CVD) method. For instance, Kumar *et al.*<sup>77</sup> obtained 2D MoS<sub>2</sub> by CVD

with MoO<sub>3</sub> powder and sulfur as precursors. The test results revealed that the MoS<sub>2</sub> gas sensor had a response time of 29 s and a recovery time of 350 s for 100 ppm concentration of NO<sub>2</sub> when operating in a RT environment irradiated by UV lamps (~365 nm). Similarly, Kim *et al.*<sup>13</sup> fabricated layer-controlled MoS<sub>2</sub> by CVD with molybdenum hexacarbonyl (Mo(CO)<sub>6</sub>) and hydrogen sulfide (H<sub>2</sub>S). It is found that the Schottky barrier changes due to the change in the number of MoS<sub>2</sub> layers, which results in an improved response of the gas sensor. Zheng *et al.*<sup>75</sup> synthesized n-type and p-type MoS<sub>2</sub> films by CVD and soft-chemistry route, respectively. In CVD process, MoO<sub>3</sub> and sulfur were used as precursors, while in the soft-chemistry route, molybdate sol-gel (contain 1% W) was used as precursors. Uniquely, they prepared a novel p-n junction gas sensor by stacking n-type and p-type MoS<sub>2</sub> atomic layers. The results represented that compared with n-type MoS<sub>2</sub> gas sensor, the p-type MoS<sub>2</sub> has a faster response to NO<sub>2</sub>. More importantly, the p-n junction sensor not only has a 20-fold increase in sensitivity to 20 ppm NO<sub>2</sub>, but also has a lower detection limit of 8 ppb.

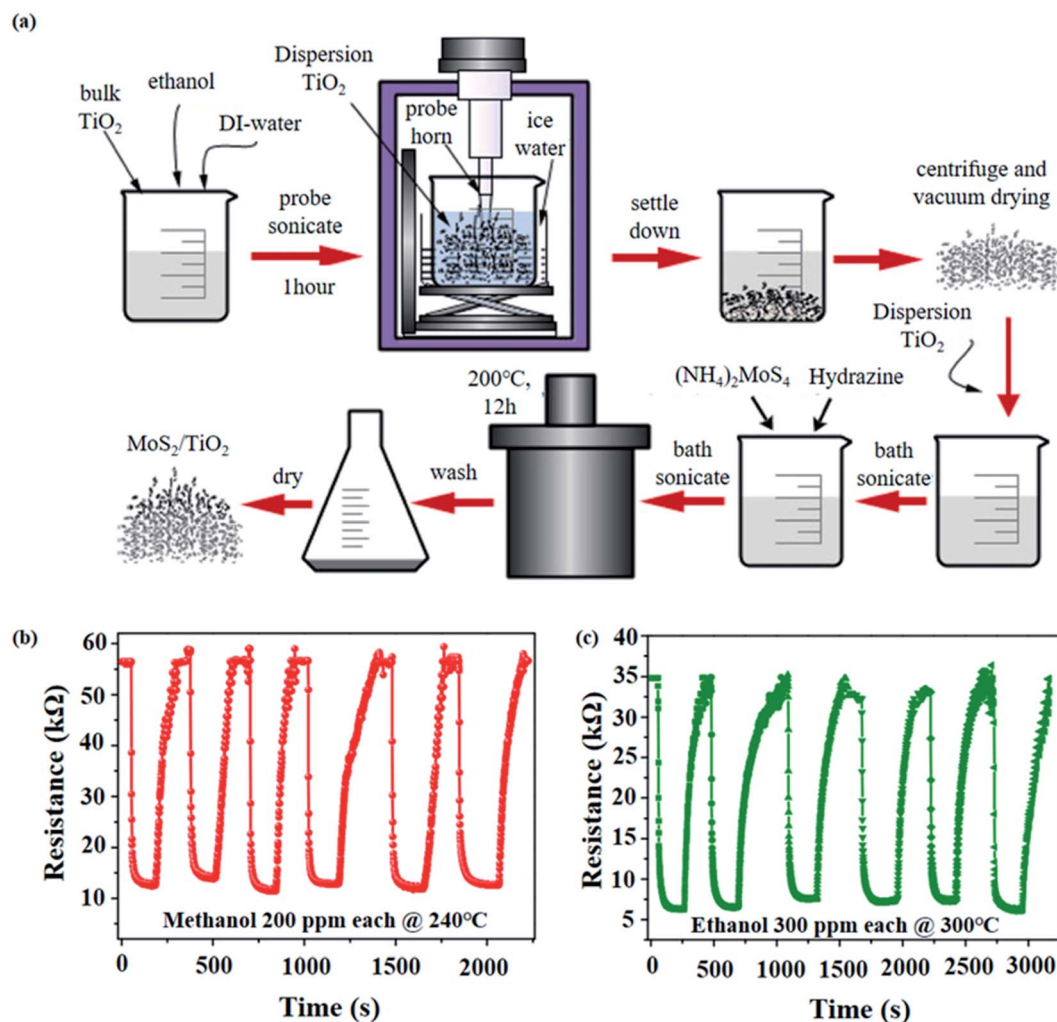


Fig. 9 (a) Schematic diagram of the synthesis of MoS<sub>2</sub>/TiO<sub>2</sub> composite.<sup>82</sup> (b) Repeatability testing of 200 ppm methanol for six consecutive cycles at an operating temperature of 240 °C.<sup>82</sup> (c) Repeatability testing of 300 ppm ethanol for six consecutive cycles at an operating temperature of 300 °C.<sup>82</sup>





Table 3 MoS<sub>2</sub>-based nanocomposites for gas sensors

| No. | Materials                          | Preparation  | Mo source   | S source   | Morphology                   | Target Gas                  | Res/Rec (s) | Response ( $R_g/R_a$ ) | T (°C)          | Detection limits                 | Ref. |
|-----|------------------------------------|--|---|--|------------------------------|-----------------------------|-------------|------------------------|-----------------|----------------------------------|------|
| 1   | MoS <sub>2</sub>                   | CVD  | MoO <sub>3</sub>                                    | Sulfur   | Film                         | 100 ppm of NO <sub>2</sub>  | 29/350      | 1.3516                 | RT (UV)         | —                                | 77   |
| 2   | MoS <sub>2</sub>                   | CVD  | Mo(CO) <sub>6</sub>                                 | H <sub>2</sub> S                                 | Film                         | 10 ppm of NO <sub>2</sub>   | —/—         | 1.6                    | RT              | —                                | 13   |
| 3   | MoS <sub>2</sub>                   | CVD  | MoO <sub>3</sub>                                    | Sulfur   | Film                         | 20 ppm of NO <sub>2</sub>   | 150/30      | —                      | RT (UV)         | 8 ppb                            | 75   |
| 4   | MoS <sub>2</sub> /PbS              | Hydrothermal method combined with chemical precipitation | Na <sub>2</sub> MoO <sub>4</sub> ·2H <sub>2</sub> O | CH <sub>3</sub> CSNH <sub>2</sub>                | Fluffy ball-like structure   | 100 ppm of NO <sub>2</sub>  | 30/235      | —                      | RT              | —                                | 78   |
| 5   | MoS <sub>2</sub> @SnO <sub>2</sub> | Electrospinning and hydrothermal growth                  | Na <sub>2</sub> MoO <sub>4</sub> ·2H <sub>2</sub> O | N <sub>2</sub> H <sub>4</sub> CS                 | Nanoflake                    | 100 ppm of NO <sub>2</sub>  | 2.2/10.54   | 0.02884                | RT              | 10 ppb                           | 79   |
| 6   | Au-MoS <sub>2</sub>                | Hydrothermal method                                      | Na <sub>2</sub> MoO <sub>4</sub> ·2H <sub>2</sub> O | CH <sub>3</sub> CSNH <sub>2</sub>                | Fluffy flower-like structure | 1 ppm of NO <sub>2</sub>    | —/27        | 8.1                    | RT (530 nm LED) | 10 ppb                           | 80   |
| 7   | MoS <sub>2</sub>                   | Micromechanical exfoliation method                       | Bulk MoS <sub>2</sub> crystal                       | Bulk MoS <sub>2</sub> crystal                    | Layered                      | 1000 ppm of NO <sub>2</sub> | —/—         | 14.72                  | RT              | —                                | 74   |
| 8   | MoS <sub>2</sub>                   | Micromechanical exfoliation method                       | Bulk MoS <sub>2</sub> crystal                       | Bulk MoS <sub>2</sub> crystal                    | Layered                      | 1000 ppm of NH <sub>3</sub> | —/—         | 1.86                   | RT              | —                                | 74   |
| 9   | SnO <sub>2</sub> /MoS <sub>2</sub> | Electrospinning and drop-coated process                  | MoS <sub>2</sub> powder                             | MoS <sub>2</sub> powder                          | Nanosheet                    | 10 ppm of SO <sub>2</sub>   | —/—         | 11.1                   | 150             | 5 ppt (parts-per-trillion)       | 81   |
| 10  | MoS <sub>2</sub> /TiO <sub>2</sub> | Low-cost hydrothermal method                             | (NH <sub>4</sub> ) <sub>2</sub> MoS <sub>4</sub>    | (NH <sub>4</sub> ) <sub>2</sub> MoS <sub>4</sub> | Layered                      | 500 ppm of ethanol          | 50/100      | nearly 0               | 300             | —                                | 82   |
| 11  | MoS <sub>2</sub> /TiO <sub>2</sub> | Low-cost hydrothermal method                             | (NH <sub>4</sub> ) <sub>2</sub> MoS <sub>4</sub>    | (NH <sub>4</sub> ) <sub>2</sub> MoS <sub>4</sub> | Layered                      | 500 ppm of methanol         | —/—         | 0.15                   | 240             | —                                | 82   |
| 12  | CuO/rGO                            | LbL self-assembly  | —   | —  | —                            | 1 ppm of CO                 | 70/160      | 1.0256                 | RT              | —                                | 83   |
| 13  | Single-walled carbon nanotubes     | —  | —   | —  | —                            | 100 ppb of NO               | —/—         | 0.7136                 | RT              | —                                | 84   |
| 14  | Graphene oxide                     | Thermal reduction  | —   | —  | —                            | 5 ppm of NO <sub>2</sub>    | —/—         | 0.83                   | RT              | —                                | 85   |
| 15  | DETA doped graphene                | CVD and vapor-phase molecular doping                     | —   | —  | —                            | 50 ppm of NO <sub>2</sub>   | —/—         | 0.23                   | RT              | 0.83 ppq (parts per quadrillion) | 86   |

Just as pure MoS<sub>2</sub> gas sensors exhibit gas-sensitive performance on NO<sub>2</sub> gas, MoS<sub>2</sub> composite gas sensors also have excellent gas-sensitive properties. For example, the PbS quantum dots modified MoS<sub>2</sub> (MoS<sub>2</sub>/PbS) composite gas sensor prepared by Xin *et al.*<sup>78</sup> has excellent gas-sensitive performance for NO<sub>2</sub> due to the high response of PbS quantum dots to NO<sub>2</sub> and the prevention of MoS<sub>2</sub> oxidation. MoS<sub>2</sub>/PbS was prepared by hydrothermal and chemical precipitation methods, and the specific preparation is shown in Fig. 6a. First of all, pure MoS<sub>2</sub> was prepared from Na<sub>2</sub>MoO<sub>4</sub>·2H<sub>2</sub>O and CH<sub>3</sub>CSNH<sub>2</sub> by hydrothermal reaction under an Teflon-lined autoclave at 200 °C. Secondly, the doping of PbS quantum dots was achieved by chemical precipitation using Na<sub>2</sub>S·9H<sub>2</sub>O and Pb(NO<sub>3</sub>)<sub>2</sub> as precursors. Compared with pure MoS<sub>2</sub>, the MoS<sub>2</sub>/PbS gas sensor has higher response and recovery performance for 100 ppm NO<sub>2</sub> gas at RT (Fig. 6b).

Composites of MoS<sub>2</sub> nanosheets with SnO<sub>2</sub> nanotubes were prepared for gas-sensitive properties by Bai *et al.* MoS<sub>2</sub>@SnO<sub>2</sub> heterostructure exhibits impressive sensitivity and selectivity for the detection of NO<sub>2</sub> gas at RT. Tests illustrated that the MoS<sub>2</sub>@SnO<sub>2</sub> gas sensor had a fast response time (2.2 s), a short recovery time (10.54 s), a low detection limit (10 ppb) and excellent stability (20 weeks) (Fig. 7a).<sup>79</sup> Another reported composite is MoS<sub>2</sub> nanoflowers modified with Au nanoparticles prepared by Chen *et al.* Surprisingly, the Au–MoS<sub>2</sub> gas sensor exhibits an extremely low detection limit (10 ppb) for NO<sub>2</sub> at RT with strong resistance to moisture interference under 530 nm light illumination (Fig. 7b).<sup>80</sup>

The preparation of MoS<sub>2</sub>@SnO<sub>2</sub> was achieved by electrostatic spinning and hydrothermal methods, as presented in Fig. 7c. First, stannous chloride (SnCl<sub>2</sub>·2H<sub>2</sub>O) was mixed with anhydrous ethanol, DMF and PVP to make electrospinning solution, and SnO<sub>2</sub> NTs were obtained by spinning technique and subsequent high-temperature calcination treatment. Second, N<sub>2</sub>H<sub>4</sub>CS and Na<sub>2</sub>MoO<sub>4</sub>·2H<sub>2</sub>O were used as the S and Mo sources, respectively, to mix with the previously prepared SnO<sub>2</sub> NTs, and the reaction was carried out in an autoclave at 200 °C to realize MoS<sub>2</sub> on SnO<sub>2</sub> NTs growth.<sup>79</sup>

The fabrication of Au–MoS<sub>2</sub> composites was achieved by a two-step hydrothermal method. Firstly, MoS<sub>2</sub> was obtained by reacting Na<sub>2</sub>MoO<sub>4</sub>·2H<sub>2</sub>O and thioacetamide (CH<sub>3</sub>CSNH<sub>2</sub>) in a Teflon-lined autoclave at 200 °C for 36 h. Secondly, Au–MoS<sub>2</sub> was synthesized by mixing sodium citrate tribasic dihydrate (C<sub>6</sub>H<sub>5</sub>Na<sub>3</sub>O<sub>7</sub>·2H<sub>2</sub>O), tannic acid (C<sub>76</sub>H<sub>52</sub>O<sub>46</sub>) and previously prepared MoS<sub>2</sub>, then adding gold chloride trihydrate (HAuCl<sub>4</sub>·3H<sub>2</sub>O) solution dropwise and stirring well, and then reacting in a Teflon-lined autoclave.<sup>80</sup>

## 4.2 MoS<sub>2</sub>-based gas sensors for other gases

The MoS<sub>2</sub>-based gas sensors not only detect NO<sub>2</sub> gas extremely well, but also reveal excellent gas sensitivity to NH<sub>3</sub>, SO<sub>2</sub> and alcohol gases.

Dattatray J. Late *et al.*<sup>74</sup> prepared layered MoS<sub>2</sub> films by micromechanical exfoliation method in 2013 for the preparation of gas sensors to detect NH<sub>3</sub> gas. The experimental results demonstrated that the 2-layer MoS<sub>2</sub> and 5-layer MoS<sub>2</sub> have

excellent gas-sensitive performance to NH<sub>3</sub>, and the 5-layer MoS<sub>2</sub> is more sensitive to detect NH<sub>3</sub>. In addition, when the MoS<sub>2</sub> gas sensor is applied with a positive gate voltage, the electric field formed at the interface will repel the electrons given by NH<sub>3</sub> as an electron donor, resulting in a decrease in the sensitivity of MoS<sub>2</sub> to NH<sub>3</sub>. Fig. 8a shows the curves of sensitivity with NH<sub>3</sub> concentration for 2-layer and 5-layer MoS<sub>2</sub> with and without gate voltage.

Nguyen Ngoc Viet *et al.*<sup>81</sup> prepared MoS<sub>2</sub>/SnO<sub>2</sub> sensors for SO<sub>2</sub> gas detection by on-chip electrostatic spinning and subsequently dropping MoS<sub>2</sub> nanosheets-dispersed solution, and the fabrication is depicted in Fig. 8b. The test results indicated that the MoS<sub>2</sub>/SnO<sub>2</sub> gas sensor had good gas-sensitive performance for 10 ppm SO<sub>2</sub> gas at 150 °C (Fig. 8c).

Sukhwinder Singh *et al.*<sup>82</sup> prepared MoS<sub>2</sub>/TiO<sub>2</sub> composite for the detection of methanol and ethanol. As shown in Fig. 9a, MoS<sub>2</sub>/TiO<sub>2</sub> hybrid was obtained by two steps: first, pure TiO<sub>2</sub> powder was mixed with ethanol and other solvents for probe sonication, and second, (NH<sub>4</sub>)<sub>2</sub>MoS<sub>4</sub> was mixed with the produced TiO<sub>2</sub> suspension to prepare MoS<sub>2</sub>/TiO<sub>2</sub> composites by hydrothermal method. The test results revealed that the best working temperatures of MoS<sub>2</sub>/TiO<sub>2</sub> composites for methanol and ethanol were 240 °C and 300 °C, respectively, and more importantly, the MoS<sub>2</sub>/TiO<sub>2</sub> sensor had good response and better stability (Fig. 9b and c).

The gas sensing performance of MoS<sub>2</sub>-based nanomaterials and the preparation methods are listed in Table 3. As a comparison, the gas-sensitive properties of some typical materials are collected at the end of the table.<sup>83–86</sup>

## 5. Conclusion

This review highlights recent advances in MoS<sub>2</sub>-based materials synthesis and their applications toward batteries, catalysts and gas sensors. First of all, MoS<sub>2</sub>, due to the large specific surface area and abundant active sites, has become one of the most popular electrode materials. In addition, the compound of MoS<sub>2</sub> with CNFs and TiO<sub>2</sub> materials overcomes the inherent defects of MoS<sub>2</sub> and greatly improves the electrochemical performance of the battery. Second, MoS<sub>2</sub> has catalytic active sites on the edges, which makes it one of the most popular candidates to replace noble metal catalysts. The composite of MoS<sub>2</sub> with MoN, CoS<sub>2</sub> and C<sub>3</sub>N<sub>4</sub> improved the catalytic performance of the catalyst. Finally, MoS<sub>2</sub> can be used in gas sensors due to the semiconductor properties and non-zero forbidden bandwidth. The compound of MoS<sub>2</sub> with materials such as SnO<sub>2</sub> and PbS can enhance the sensitivity of the gas sensor to the gas to be detected and reduce the detection limit.

It is worth noting that while MoS<sub>2</sub> has made good progress in these areas, challenges remain in its future development. First, MoS<sub>2</sub> has low electrical conductivity and multilayer MoS<sub>2</sub> tends to accumulate and aggregate in the preparation, which is not conducive to electron transport. Second, the active sites of MoS<sub>2</sub> are mainly at the edges but not at the basal plane, which has a significant impact on both the sensing performance and catalytic performance. Therefore, it is necessary to further explore the compounding of MoS<sub>2</sub> with other materials or to

optimize the structure of MoS<sub>2</sub> (e.g., preparation of MoS<sub>2</sub> NTs, etc.). In addition, 1T-MoS<sub>2</sub> has better electrical conductivity compared with 2H-MoS<sub>2</sub>, and there are also interesting electrical properties using 1T-MoS<sub>2</sub> compounded with other materials.

In a word, MoS<sub>2</sub> has promising applications in energy and gas sensors due to its excellent and unique physicochemical properties. We believe that with the joint efforts of researchers in the future, better progress will be made in the applications and synthesis of MoS<sub>2</sub>.

## Conflicts of interest

There are no conflicts to declare.

## Acknowledgements

This work was supported by the National Science Foundation of China (No. 61904123), the Natural Science Foundation of Tianjin (No. 18JCQNJC71800), Scientific Research Project of Tianjin Educational Committee (No. 2018KJ220), Tianjin Technical and Engineering Center of Nonwovens (No. KF202103).

## References

- 1 K. S. Novoselov, D. Jiang, F. Schedin, T. Booth, V. Khotkevich, S. Morozov and A. K. Geim, *Proc. Natl. Acad. Sci.*, 2005, **102**, 10451–10453.
- 2 S. Z. Butler, S. M. Hollen, L. Cao, Y. Cui, J. A. Gupta, H. R. Gutiérrez, T. F. Heinz, S. S. Hong, J. Huang and A. F. Ismach, *ACS Nano*, 2013, **7**, 2898–2926.
- 3 G. R. Bhimanapati, Z. Lin, V. Meunier, Y. Jung, J. Cha, S. Das, D. Xiao, Y. Son, M. S. Strano and V. R. Cooper, *ACS Nano*, 2015, **9**, 11509–11539.
- 4 Z. Wang and B. Mi, *Environ. Sci. Technol.*, 2017, **51**, 8229–8244.
- 5 H. Wang, C. Li, P. Fang, Z. Zhang and J. Z. Zhang, *Chem. Soc. Rev.*, 2018, **47**, 6101–6127.
- 6 U. Krishnan, M. Kaur, K. Singh, M. Kumar and A. Kumar, *Superlattices Microstruct.*, 2019, **128**, 274–297.
- 7 T. Nawz, A. Safdar, M. Hussain, D. Sung Lee and M. Siyar, *Crystals*, 2020, **10**.
- 8 D. Saha and P. Kruse, *J. Electrochem. Soc.*, 2020, **167**.
- 9 O. Samy and A. El Moutaouakil, *Energies*, 2021, **14**.
- 10 Y. Zhang, H. Tao, S. Du and X. Yang, *ACS Appl. Mater. Interfaces*, 2019, **11**, 11327–11337.
- 11 R. Bose, Z. Jin, S. Shin, S. Kim, S. Lee and Y. S. Min, *Langmuir*, 2017, **33**, 5628–5635.
- 12 Y. Wang, J. Sunarso, F. Wang, B. Zhao, X. Liu and G. Chen, *Ceram. Int.*, 2017, **43**, 11028–11033.
- 13 Y. Kim, S. K. Kang, N. C. Oh, H. D. Lee, S. M. Lee, J. Park and H. Kim, *ACS Appl. Mater. Interfaces*, 2019, **11**, 38902–38909.
- 14 Z. Liu, L. Zhao, Y. Liu, Z. Gao, S. Yuan, X. Li, N. Li and S. Miao, *Appl. Catal., B*, 2019, **246**, 296–302.
- 15 E. Singh, K. S. Kim, G. Y. Yeom and H. S. Nalwa, *ACS Appl. Mater. Interfaces*, 2017, **9**, 3223–3245.
- 16 X. Li and H. Zhu, *J. Materiomics*, 2015, **1**, 33–44.
- 17 Y. Qiao, T. Hirtz, F. Wu, G. Deng, X. Li, Y. Zhi, H. Tian, Y. Yang and T.-L. Ren, *ACS Appl. Electron. Mater.*, 2019, **2**, 346–370.
- 18 Y. Liu and F. Gu, *Nanoscale Adv.*, 2021, **3**, 2117–2138.
- 19 O. Samy, S. Zeng, M. D. Birowosuto and A. El Moutaouakil, *Crystals*, 2021, **11**.
- 20 Y. P. Venkata Subbaiah, K. J. Saji and A. Tiwari, *Adv. Funct. Mater.*, 2016, **26**, 2046–2069.
- 21 W. Zhang, P. Zhang, Z. Su and G. Wei, *Nanoscale*, 2015, **7**, 18364–18378.
- 22 H. S. Nalwa, *RSC Adv.*, 2020, **10**, 30529–30602.
- 23 S. Barua, H. S. Dutta, S. Gogoi, R. Devi and R. Khan, *ACS Appl. Nano Mater.*, 2017, **1**, 2–25.
- 24 S. Shi, Z. Sun and Y. H. Hu, *J. Mater. Chem. A*, 2018, **6**, 23932–23977.
- 25 L. Lei, D. Huang, G. Zeng, M. Cheng, D. Jiang, C. Zhou, S. Chen and W. Wang, *Coord. Chem. Rev.*, 2019, **399**, 213020.
- 26 Y. Jiao, A. M. Hafez, D. Cao, A. Mukhopadhyay, Y. Ma and H. Zhu, *Small*, 2018, **14**, e1800640.
- 27 J. Sun, X. Li, W. Guo, M. Zhao, X. Fan, Y. Dong, C. Xu, J. Deng and Y. Fu, *Crystals*, 2017, **7**(7), 198.
- 28 Z. Liu, X. Wang, Z. Liu, S. Zhang, Z. Lv, Y. Cui, L. Du, K. Li, G. Zhang, M. C. Lin and H. Du, *ACS Appl. Mater. Interfaces*, 2021, **13**, 28164–28170.
- 29 N. Qiu, Z. Yang, R. Xue, Y. Wang, Y. Zhu and W. Liu, *Nano Lett.*, 2021, **21**, 2738–2744.
- 30 S. G. Stolyarova, A. A. Kotsun, Y. V. Shubin, V. O. Koroteev, P. E. Plyusnin, Y. L. Mikhlin, M. S. Mel'gunov, A. V. Okotrub and L. G. Bulusheva, *ACS Appl. Energy Mater.*, 2020, **3**, 10802–10813.
- 31 Z. Yuan, L. Wang, D. Li, J. Cao and W. Han, *ACS Nano*, 2021, **15**, 7439–7450.
- 32 C. Zhu, X. Mu, P. A. van Aken, Y. Yu and J. Maier, *Angew. Chem., Int. Ed. Engl.*, 2014, **53**, 2152–2156.
- 33 C.-Y. Wei, P.-C. Lee, C.-W. Tsao, L.-H. Lee, D.-Y. Wang and C.-Y. Wen, *ACS Appl. Energy Mater.*, 2020, **3**, 7066–7072.
- 34 H. Wu, C. Hou, G. Shen, T. Liu, Y. Shao, R. Xiao and H. Wang, *Nano Res.*, 2018, **11**, 5866–5878.
- 35 J. Zhang, Y. Li, T. Gao, X. Sun, P. Cao and G. Zhou, *Ceram. Int.*, 2018, **44**, 8550–8555.
- 36 X. Zhao, Z. Liu, W. Xiao, H. Huang, L. Zhang, Y. Cheng and J. Zhang, *ACS Appl. Nano Mater.*, 2020, **3**, 7580–7586.
- 37 S. Ding, D. Zhang, J. S. Chen and X. W. Lou, *Nanoscale*, 2012, **4**, 95–98.
- 38 Y. Lu, X. Yao, J. Yin, G. Peng, P. Cui and X. Xu, *RSC Adv.*, 2015, **5**, 7938–7943.
- 39 K. Yao, Z. Xu, J. Huang, M. Ma, L. Fu, X. Shen, J. Li and M. Fu, *Small*, 2019, **15**, e1805405.
- 40 A. Cheng, H. Zhang, W. Zhong, Z. Li, Y. Tang and Z. Li, *J. Electroanal. Chem.*, 2019, **843**, 31–36.
- 41 L. Han, S. Wu, Z. Hu, M. Chen, J. Ding, S. Wang, Y. Zhang, D. Guo, L. Zhang, S. Cao and S. Chou, *ACS Appl. Mater. Interfaces*, 2020, **12**, 10402–10409.
- 42 Q. Pan, Q. Zhang, F. Zheng, Y. Liu, Y. Li, X. Ou, X. Xiong, C. Yang and M. Liu, *ACS Nano*, 2018, **12**, 12578–12586.



- 43 Y. Zhang, H. Tao, T. Li, S. Du, J. Li, Y. Zhang and X. Yang, *ACS Appl. Mater. Interfaces*, 2018, **10**, 35206–35215.
- 44 H. Dai, M. Tang, J. Huang and Z. Wang, *ACS Appl. Mater. Interfaces*, 2021, **13**, 10870–10877.
- 45 Y. Zhang, H. Tao, S. Du and X. Yang, *ACS Appl. Mater. Interfaces*, 2019, **11**, 11327–11337.
- 46 H. Dai, J. Sun, Y. Zhou, Z. Zhou, W. Luo, G. Wei and H. Deng, *ACS Sustainable Chem. Eng.*, 2020, **8**, 8102–8110.
- 47 Z. Li, B. Niu, J. Liu, J. Li and F. Kang, *ACS Appl. Mater. Interfaces*, 2018, **10**, 9451–9459.
- 48 W. Yang, H. Lu, Y. Cao, B. Xu, Y. Deng and W. Cai, *ACS Sustainable Chem. Eng.*, 2019, **7**, 4861–4867.
- 49 S. Guo, H. Yang, M. Liu, X. Feng, H. Xu, Y. Bai and C. Wu, *ACS Appl. Energy Mater.*, 2021, **4**, 7064–7072.
- 50 Z. Sheng, P. Qi, Y. Lu, G. Liu, M. Chen, X. Gan, Y. Qin, K. Hao and Y. Tang, *ACS Appl. Mater. Interfaces*, 2021, **13**, 34495–34506.
- 51 A. C. M. de Moraes, W. J. Hyun, N. S. Luu, J. M. Lim, K. Y. Park and M. C. Hersam, *ACS Appl. Mater. Interfaces*, 2020, **12**, 8107–8114.
- 52 G. Zhang, K. Lin, X. Qin, L. Zhang, T. Li, F. Lv, Y. Xia, W. Han, F. Kang and B. Li, *ACS Appl. Mater. Interfaces*, 2020, **12**, 37034–37046.
- 53 P. Hei, S. Luo, K. Wei, J. Zhou, Y. Zhao and F. Gao, *ACS Sustainable Chem. Eng.*, 2020, **9**, 216–223.
- 54 H. Liang, Z. Cao, F. Ming, W. Zhang, D. H. Anjum, Y. Cui, L. Cavallo and H. N. Alshareef, *Nano Lett.*, 2019, **19**, 3199–3206.
- 55 L. Jia, B. Liu, Y. Zhao, W. Chen, D. Mou, J. Fu, Y. Wang, W. Xin and L. Zhao, *J. Mater. Sci.*, 2020, **55**, 16197–16210.
- 56 D. Wang, X. Zhang, S. Bao, Z. Zhang, H. Fei and Z. Wu, *J. Mater. Chem. A*, 2017, **5**, 2681–2688.
- 57 X. Han, X. Tong, X. Liu, A. Chen, X. Wen, N. Yang and X.-Y. Guo, *ACS Catal.*, 2018, **8**, 1828–1836.
- 58 Y.-J. Yuan, P. Wang, Z. Li, Y. Wu, W. Bai, Y. Su, J. Guan, S. Wu, J. Zhong, Z.-T. Yu and Z. Zou, *Appl. Catal., B*, 2019, **242**, 1–8.
- 59 X.-L. Yin, G.-Y. He, B. Sun, W.-J. Jiang, D.-J. Xue, A.-D. Xia, L.-J. Wan and J.-S. Hu, *Nano Energy*, 2016, **28**, 319–329.
- 60 Q. Li, W. Liu, L. Xiao, X. Chen and X. Xu, *Mater. Lett.*, 2021, **285**.
- 61 J. Wang, W. Fang, Y. Hu, Y. Zhang, J. Dang, Y. Wu, H. Zhao and Z. Li, *Catal. Sci. Technol.*, 2020, **10**, 154–163.
- 62 A. Wu, Y. Gu, Y. Xie, H. Yan, Y. Jiao, D. Wang and C. Tian, *J. Alloys Compd.*, 2021, 867.
- 63 H. Zhu, F. Lyu, M. Du, M. Zhang, Q. Wang, J. Yao and B. Guo, *ACS Appl. Mater. Interfaces*, 2014, **6**, 22126–22137.
- 64 Y. Zhu, L. Song, N. Song, M. Li, C. Wang and X. Lu, *ACS Sustainable Chem. Eng.*, 2019, **7**, 2899–2905.
- 65 D. Xie, G. Yang, D. Yu, Y. Hao, S. Han, Y. Cheng, F. Hu, L. Li, H. Wei, C. Ji and S. Peng, *ACS Sustainable Chem. Eng.*, 2020, **8**, 14179–14189.
- 66 S. Bawari, N. M. Kaley, S. Pal, T. V. Vineesh, S. Ghosh, J. Mondal and T. N. Narayanan, *Phys. Chem. Chem. Phys.*, 2018, **20**, 15007–15014.
- 67 Q. Zhang, Z. Duan, M. Li and J. Guan, *Chem. Commun.*, 2020, **56**, 794–797.
- 68 X. Hu, S. Lu, J. Tian, N. Wei, X. Song, X. Wang and H. Cui, *Appl. Catal., B*, 2019, **241**, 329–337.
- 69 B. Sun, W. Zhou, H. Li, L. Ren, P. Qiao, W. Li and H. Fu, *Adv. Mater.*, 2018, **30**, e1804282.
- 70 Y.-J. Yuan, Z. Shen, S. Wu, Y. Su, L. Pei, Z. Ji, M. Ding, W. Bai, Y. Chen, Z.-T. Yu and Z. Zou, *Appl. Catal., B*, 2019, **246**, 120–128.
- 71 H. Zhao, Z. Jiang, K. Xiao, H. Sun, H. S. Chan, T. H. Tsang, S. Yang and P. K. Wong, *Appl. Catal., B*, 2021, 280.
- 72 G. Zhao, A. Wang, W. He, Y. Xing and X. Xu, *Adv. Mater. Interfaces*, 2019, **6**, 1900062.
- 73 N. Qin, J. Xiong, R. Liang, Y. Liu, S. Zhang, Y. Li, Z. Li and L. Wu, *Appl. Catal., B*, 2017, **202**, 374–380.
- 74 D. J. Late, Y. K. Huang, B. Liu, J. Acharya, S. N. Shirodkar, J. Luo, A. Yan, D. Charles, U. V. Waghmare and V. P. Dravid, *ACS Nano*, 2013, **7**, 4879–4891.
- 75 W. Zheng, Y. Xu, L. Zheng, C. Yang, N. Pinna, X. Liu and J. Zhang, *Adv. Funct. Mater.*, 2020, **30**, 2000435.
- 76 T. Pham, G. Li, E. Bekyarova, M. E. Itkis and A. Mulchandani, *ACS Nano*, 2019, **13**, 3196–3205.
- 77 R. Kumar, N. Goel and M. Kumar, *ACS Sens.*, 2017, **2**, 1744–1752.
- 78 X. Xin, Y. Zhang, X. Guan, J. Cao, W. Li, X. Long and X. Tan, *ACS Appl. Mater. Interfaces*, 2019, **11**, 9438–9447.
- 79 X. Bai, H. Lv, Z. Liu, J. Chen, J. Wang, B. Sun, Y. Zhang, R. Wang and K. Shi, *J. Hazard. Mater.*, 2021, **416**, 125830.
- 80 P. Chen, J. Hu, M. Yin, W. Bai, X. Chen and Y. Zhang, *ACS Appl. Nano Mater.*, 2021, **4**, 5981–5991.
- 81 N. N. Viet, L. V. Thong, T. K. Dang, P. H. Phuoc, N. H. Chien, C. M. Hung, N. D. Hoa, N. Van Duy, N. Van Toan, N. T. Son and N. Van Hieu, *Anal. Chim. Acta*, 2021, **1167**, 338576.
- 82 S. Singh and S. Sharma, *Sens. Actuators, B*, 2022, 350.
- 83 D. Zhang, C. Jiang, J. Liu and Y. Cao, *Sens. Actuators, B*, 2017, **247**, 875–882.
- 84 D.-W. Jeong, K. H. Kim, B. S. Kim and Y. T. Byun, *Appl. Surf. Sci.*, 2021, 550.
- 85 Y. R. Choi, Y.-G. Yoon, K. S. Choi, J. H. Kang, Y.-S. Shim, Y. H. Kim, H. J. Chang, J.-H. Lee, C. R. Park, S. Y. Kim and H. W. Jang, *Carbon*, 2015, **91**, 178–187.
- 86 B. Kwon, H. Bae, H. Lee, S. Kim, J. Hwang, H. Lim, J. H. Lee, K. Cho, J. Ye, S. Lee and W. H. Lee, *ACS Nano*, 2022, **16**, 2176–2187.

